REVIEW ARTICLE

Real-Time Magnetic Resonance Imaging

Krishna S. Nayak, PhD,[1*] Yongwan Lim, PhD,[1] Adrienne E. Campbell-Washburn, PhD,[2] and Jennifer Steeden, PhD[3]

Real-time magnetic resonance imaging (RT-MRI) allows for imaging dynamic processes as they occur, without relying on any repetition or synchronization. This is made possible by modern MRI technology such as fast-switching gradients and parallel imaging. It is compatible with many (but not all) MRI sequences, including spoiled gradient echo, balanced steady-state free precession, and single-shot rapid acquisition with relaxation enhancement. RT-MRI has earned an important role in both diagnostic imaging and image guidance of invasive procedures. Its unique diagnostic value is prominent in areas of the body that undergo substantial and often irregular motion, such as the heart, gastrointestinal system, upper airway vocal tract, and joints. Its value in interventional procedure guidance is prominent for procedures that require multiple forms of soft-tissue contrast, as well as flow information. In this review, we discuss the history of RT-MRI, fundamental tradeoffs, enabling technology, established applications, and current trends.
Level of Evidence: 5
Technical Efficacy Stage: 1

J. MAGN. RESON. IMAGING 2022;55:81–99.

REAL-TIME MAGNETIC RESONANCE IMAGING (RT-MRI) enables rapid and continuous acquisition of images that allows visualization of dynamic processes as they occur. RT-MRI does not rely on any gating, synchronization, or repetition of the underlying movement or contrast dynamics. The quality of RT-MRI has experienced major leaps in the past 30+ years due to advances in MRI technology, including fast switching gradients, array receiver coils, and advanced reconstruction including parallel imaging, compressed sensing, and artificial intelligence. Over this same time window, RT-MRI has earned a substantial role in both diagnostic imaging and in the image guidance of invasive procedures. Diagnostic RT-MRI has proven most valuable in areas of the body that undergo substantial and irregular motion, such as the heart (eg, arrhythmia), upper airway vocal tract (eg, speech production), joints (eg, instability), and gastrointestinal system (eg, motility). RT-MRI for interventional guidance has proven most valuable for procedures that require multiple forms of soft-tissue contrast, as well as flow information (eg, right heart catheterization).

Historically, MRI has had a reputation of being a "slow" modality, especially compared to x-ray, computed tomography (CT), and ultrasound. This perception is changing. On modern commercial MRI equipment, RT-MRI is now feasible, practical, and readily available. It is compatible with most MRI sequences, and notably includes proton density (PD) and T_1-weighted (T_1w) spoiled gradient echo (GRE), balanced steady-state free precession (bSSFP), and single-shot rapid acquisition with relaxation enhancement (RARE). RT-MRI can provide more than adequate spatiotemporal resolution, contrast-to-noise efficiency, and image quality for a wide array of applications.

The purpose of this review is to summarize current state-of-the-art RT-MRI technology and clinical applications, predominantly focusing on imaging of dynamic motion. We begin with a discussion of the history of RT-MRI and fundamental tradeoffs. We then review enabling technology, which includes hardware, acquisition, reconstruction, interaction, and postprocessing. Next, we review the most common applications, including cardiac, interventional, upper airway, and

View this article online at wileyonlinelibrary.com. DOI: 10.1002/jmri.27411

Received Aug 1, 2020, Accepted for publication Oct 9, 2020.

*Address reprint requests to: K.S.N., 3740 McClintock Ave, EEB 400C, Los Angeles, CA 90089-2564, USA. E-mail: knayak@usc.edu

From the [1]Ming Hsieh Department of Electrical and Computer Engineering, University of Southern California, Los Angeles, California, USA; [2]Cardiovascular Branch, Division of Intramural Research, National Heart, Lung and Blood Institute, National Institutes of Health, Bethesda, Maryland, USA; and [3]Institute of Cardiovascular Science, Centre for Cardiovascular Imaging, University College London, London, UK

Additional supporting information may be found in the online version of this article

musculoskeletal. Finally, we discuss current trends, including the use of machine learning and the use of high-performance low-field MRI systems.

There has been some recent debate regarding the nomenclature for RT-MRI.[1,2] In this article, *RT-MRI* will refer to real-time acquisition that does not use any gating, synchronization, or repetition of the movement. We use the term *interactive RT-MRI* when latency between acquisition and image display is short enough to permit interaction (eg, guidance of interventions, or calculation of real-time cardiac output).

Brief History

Real-time techniques are commonly used in medical imaging, including live video for gait analysis, fluoroscopy for diagnostic studies of the gastrointestinal tract, and ultrasound to guide interventional procedures such as biopsies. Development toward fast MRI began shortly after the first medical applications. This included the development of echo planar imaging (EPI) by Sir Peter Mansfield in 1977,[3] as well as introduction of fast low angle shot magnetic resonance imaging (FLASH) by Frahm et al in 1986,[4] and fast spin-echo imaging (RARE) by Hennig et al in 1986.[5] Early clinical applications of real-time imaging include MR fluoroscopic images of the head by Farzaneh et al in 1989,[6] followed by techniques to interactively control scan slice orientation and image contrast by Holzinger et al in 1990,[7] and real-time flow measurements by Riederer et al in 1991.[8]

More recent developments have enabled substantial progress in MRI acquisition speed, which are discussed below. There has been tremendous growth in the number of publications on RT-MRI, as shown in Fig. 1. Many of the large vendors have adopted the use of interactive RT-MRI for localization and scan plane/volume prescription. And several diagnostic and interventional applications have developed and matured.

Fundamental Tradeoffs

MRI in general must balance a tradeoff between spatial resolution, temporal resolution, signal-to-noise ratio (SNR), artifacts, reconstruction latency, and modeling assumptions. This tradeoff is put to the test in RT-MRI, where temporal resolution is at a premium. Figure 2 shows a scatterplot of spatial resolution (x-axis) vs. temporal resolution (y-axis) from 22 recent publications that utilize state-of-the-art 2D RT-MRI techniques. These publications, with acquisition details listed in Table S1, were selected to include a diversity of imaging methods and target applications, and to include work from different laboratories both with and without specialized hardware and software capability. The general tradeoff is illustrated by a gray shaded bar, with fine spatial resolution and coarse temporal resolution on the upper left (eg, 1×1 mm^2 with 80 msec temporal resolution, 12.5 fps), and coarse spatial resolution and fine temporal resolution on the right (eg, 3.5×3.5 mm^2 with 20 msec temporal resolution, 50 fps). Deviations from this line occur because the data span several different applications, reconstruction methods, coil geometries, field strengths, and modeling assumptions. The impact of these is discussed in detail in the Enabling Technology section below. In general, moving towards the lower left requires using more advanced technology, advanced modeling, and increased computational demand, or accepting worse SNR and/or more severe image artifacts.

Enabling Technology

RT-MRI is made possible by several system components that are included in most modern high-end clinical MRI systems.

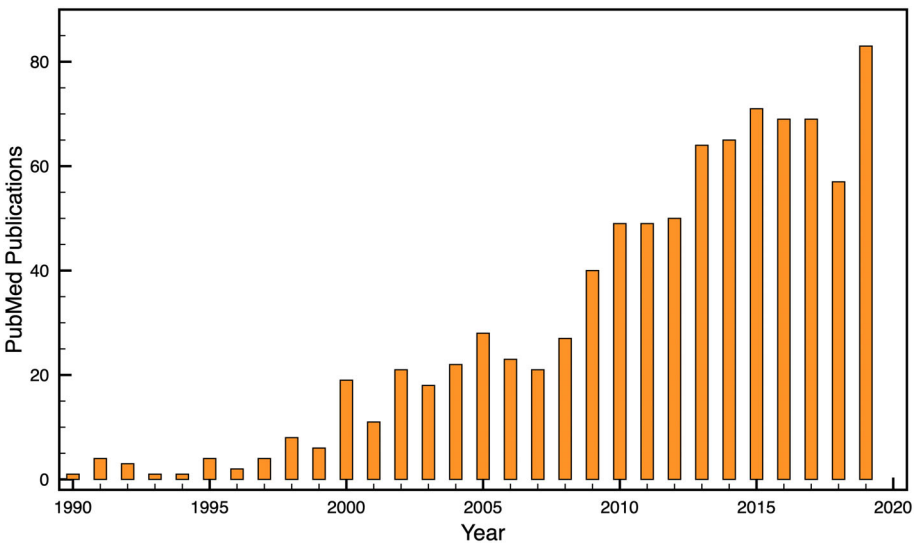

FIGURE 1: Publications involving RT-MRI. PubMed search: (("real-time MRI") OR ("real-time NMR") OR ("real-time magnetic resonance") OR ("real-time interactive MRI") OR ("RT-MRI")).

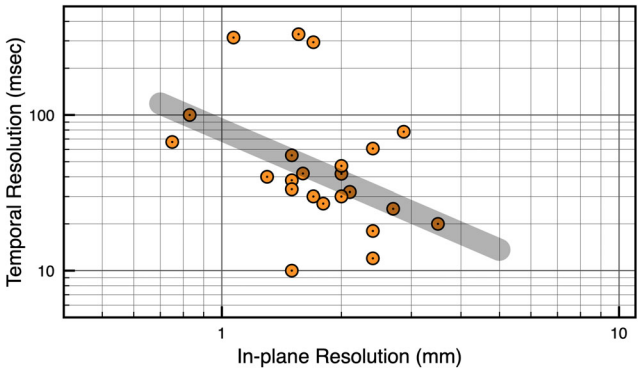

FIGURE 2: Scatterplot of 2D RT-MRI spatial and temporal resolution. Spatial resolution (x-axis) vs. temporal resolution (y-axis) is plotted from 22 recent publications that utilize state-of-the-art methodology, as selected by the authors of this review, summarized in Table S1. The gray shaded bar indicates the general spatiotemporal resolution tradeoff. All substantial deviations are due to variations in the FOV, use of parallel imaging, use of reconstruction constraints, and minimum acceptable SNR.

These beneficial components are discussed in this section. Items that are nonstandard are clearly identified.

Hardware

The speed of MRI is fundamentally limited by nuclear magnetic resonance (NMR) relaxation, and the time required to cover *k*-space. RT-MRI therefore relies on time-efficient spatial encoding. One major technological advance has been high-fidelity fast-switching shielded gradients, with eddy-current precompensation. Modern systems offer this with gradients that can produce ≥40 mT/m amplitude and ≥150mT/m/msec slew rate on each physical axis with a 50–100% duty cycle. This enables GRE and bSSFP contrast with very short repetition times and enables efficient *k*-space sampling (eg, spiral or echo-planar). Spiral and EPI trajectories were among the first technical advances to substantially broaden the set of applications that could be addressed with RT-MRI.[9]

RT-MRI also benefits from the use of parallel imaging, which requires carefully designed receiver coil arrays that provide diverse coil sensitivity along the likely directions of spatial encoding and *k*-space undersampling. These coils should preferably preserve body-noise dominance.[10] Several MRI manufacturers and third-party vendors manufacture such coils and optimized cardiac and torso coils are readily available. However, coils for nascent applications such as speech[11,12] and dynamic musculoskeletal imaging are not yet standardized, and there is substantial room for development.

Interactive RT-MRI requires the use of a flexible programmable console that can allow "on-the-fly" changes to the scan plane, shim, and many other imaging parameters. Several modern systems offer this capability, wherein many aspects of a pulse sequence can be modified without substantial interruption (ie, within a few milliseconds).

Data Acquisition

High frame-rate RT-MRI has been fundamentally enabled by two gradient echo sequences: GRE and bSSFP (Fig. 3a). RF-spoiled and gradient-spoiled GRE sequences are robust to artifacts and provide T_1-weighted contrast with a short repetition time (TR). bSSFP sequences[14] provide higher SNR efficiency than GRE, and provide T_2/T_1 contrast, which is extremely advantageous in cardiac imaging because of the excellent blood–myocardium contrast (Fig. 3a, right). However, bSSFP has two important limitations. One is sensitivity to off-resonance, which manifests as banding artifacts.[15] bSSFP RT-MRI is often used at ≤ 1.5T or at 3T with careful shimming over the region of interest (ROI) and with the shortest possible TR. The second issue is a transient approach to steady state, which can be problematic if the application requires frequent switching of the scan plane or volumes, or if there is flow or motion through regions that experience the banding artifact. Transient signal oscillations can be easily mitigated using catalyzation preparation schemes; however, it still takes time to reach steady-state contrast.

RT-MRI has been made possible by efficient *k*-space sampling trajectories (eg, spiral and EPI, described in the preceding section) and clever temporal undersampling schemes. Although it is inefficient, 2DFT imaging may be used in both 2D and 3D imaging due to the simplicity of reconstruction and robustness to artifacts. A wide range of $\vec{k}$ -t undersampling schemes exists for accelerated 2DFT imaging.[16–21] For example, one can use variable-density pseudo-random $\vec{k}$ -t sampling, which creates incoherent aliasing artifacts in a certain transform domain that can be resolved by advanced reconstruction algorithms.

Figure 3b illustrates more efficient sampling trajectories. EPI[3] is an alternative where multiple Cartesian lines are acquired after each excitation, therefore *k*-space can be filled only with one or fewer repetitions. However, its long readout time makes it vulnerable to ghosting and distortions from gradient waveform inaccuracy or off-resonance and near-RT correction methods[22,23] have been proposed.

Most preferred are radial and spiral samplings when higher spatial and/or temporal resolution is desired. Both spiral and radial sampling naturally oversample the center of *k*-space and this offers motion robustness and tolerance to undersampling. While radial sampling is $\pi/2$ less efficient than Cartesian, its motion robustness and tolerance to undersampling make it a popular RT-MRI acquisition method.[24] With moderate angular undersampling along with the golden angle scheme,[25] the streaking artifacts are usually mild in appearance and incoherent over time. Alternatively, spirals can be very efficient methods to cover *k*-space. Single-shot spirals can completely cover *k*-space, but the resultant long readout time increases sensitivity to off-resonance, resulting in spatial blurring. Multishot spiral

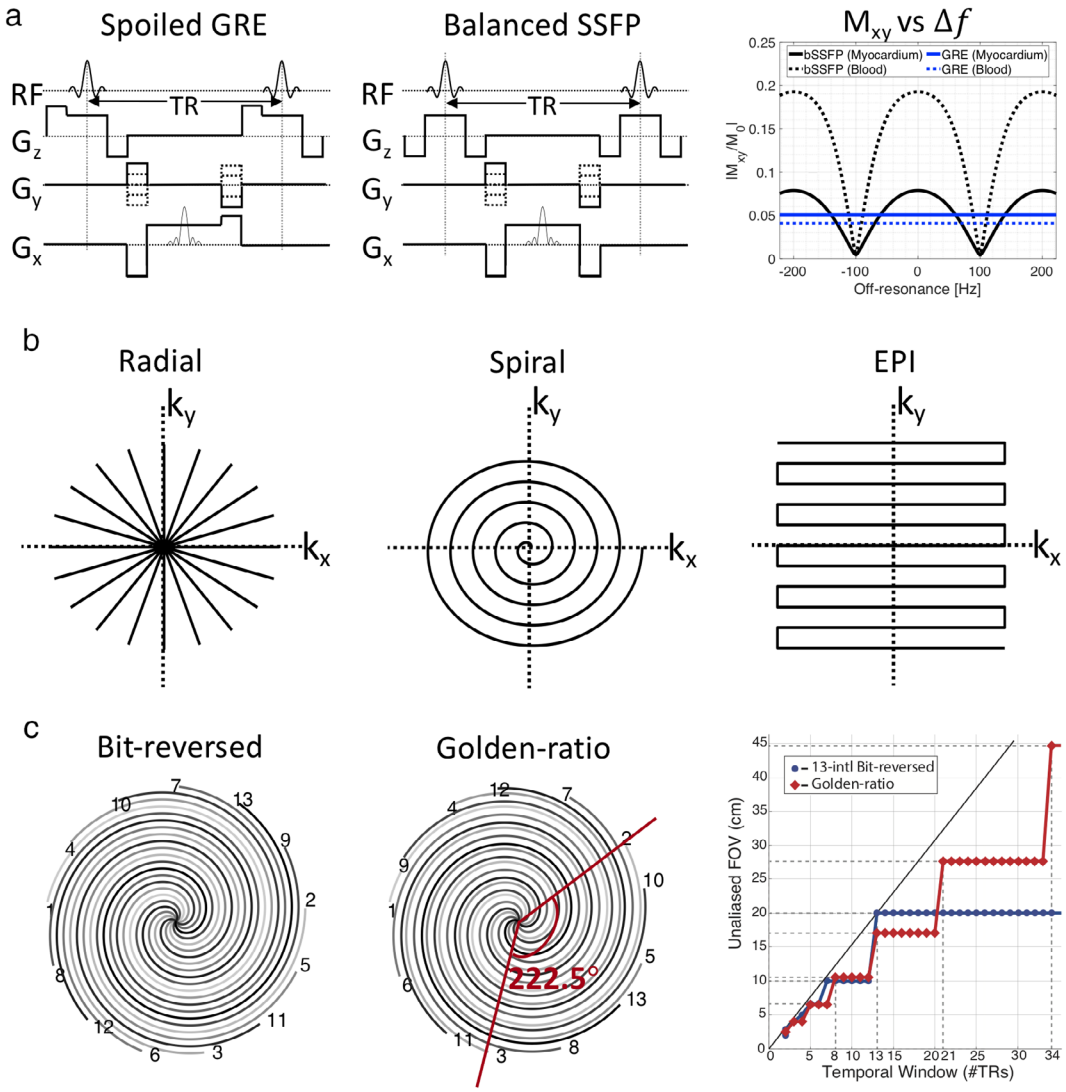

FIGURE 3: Common sequences, sampling trajectories, and view orders used in 2D RT-MRI. (a) Sequence diagrams of spoiled GRE and bSSFP, and the steady-state signal amplitude as a function of off-resonance Δf; Simulation parameters: TR = 5 msec; flip angle = 5° for spoiled GRE; flip angle = 60° for bSSFP; myocardium T_1/T_2 = 950/50 msec; blood T_1/T_2 = 1500/250 msec (representative of 1.5T). (b) Non-Cartesian sampling trajectories of undersampled radial, single-shot spiral, and single-shot EPI. (c) View orders of multishot spiral of conventional 13-interleaf bit-reversed and golden-ratio, and unaliased FOV as a function of the number of interleaves [Reproduced from Ref. (13)].

acquisitions with a short readout time can be used to alleviate blurring. Both radial and spiral imaging can be accelerated with the use of $\vec{k}$-t sampling strategies such as undersampling and random angle order schemes, for example bit-reversed[9] or golden angle[13,25] (Fig. 3c). For instance, radial or spiral imaging can be performed with an angle incremented by the golden angle (222.5°)[25] or tiny golden angles.[26] This, when undersampled, produces relatively incoherent aliasing in the spatial and temporal domain (or in a transform domain), which is well suited for advanced reconstruction algorithms. The view order is an added variable and the golden angle scheme is widely used, as it additionally has the retrospective field-of-view (FOV) tradeoff ability as opposed to the conventional scheme (right, Fig. 3c).

RT-MRI has also benefited from 2D multislice imaging,[11,27–31] which can be performed by utilizing time-interleaved sampling of acquisition schemes described above with a corresponding reduction in spatial or temporal resolution by the number of slices. Alternatively, simultaneous multislice imaging[32] can be utilized to accelerate data acquisition. Especially, controlled aliasing in parallel imaging results in higher acceleration, also known as CAIPIRINHA,[33,34] has shown substantially reduced aliasing artifacts. This technique has recently been explored in some RT-MRI studies.[35–37] 3D imaging has also been explored by extending 2D acquisition schemes to 3D or by using novel 3D sampling trajectories. Radial or spiral can readily be extended to 3D stack-of-stars[38] or 3D stack-of-spirals[39,40] by adding phase encoding steps

along k_z direction. Echo-volume imaging,[41] a 3D extension of EPI, can achieve time-efficient 3D imaging and has primarily been investigated for brain functional MRI.[42] Combinations of two sampling schemes for 3D imaging has also been explored, including EPI[43] and Cartesian sampling,[44] each combined with golden–angle radial sampling. There has also been interesting literature where volumetric image can be efficiently obtained by RT-MRI acquisitions with automatic advancement of the slice position.[45] While 3D acquisitions allow for a more flexible $\vec{k}$-t sampling strategy and therefore much redundant information to be exploited along the additional dimension, the increased amount of data is challenging in terms of data processing and reconstruction.

Reconstruction

RT-MRI data sampling and reconstruction varies with application. This is because there is a trade-off between temporal resolution and reconstruction time (governed by the complexity of the algorithm). The simplest reconstruction techniques use data sharing strategies, for example, keyhole or sliding window reconstruction.[46] This simplicity enables low latency reconstruction; however, the true temporal resolution is coarse.

Higher levels of acceleration are achievable by undersampling; however, zero-filled reconstruction results in spatial aliasing that renders the images clinically unusable. One can use parallel imaging to recover usable images, which can be performed in the image domain; sensitivity encoding (SENSE),[47] or in *k*-space; generalized autocalibrating partial parallel acquisition (GRAPPA).[48] Parallel imaging of Cartesian data enables very low latency reconstructions; hence, its popularity in RT-MRI interventional applications.

Reconstruction of undersampled non-Cartesian data is substantially more complex. This is because the *k*-space points must be resampled onto a Cartesian grid in order to use the fast Fourier transform (FFT), which increases computation demand.[49] Additionally, in non-Cartesian SENSE each voxel in the image domain can potentially alias with all of the other voxels, resulting in the need for time-consuming iterative reconstructions.[50] In non-Cartesian GRAPPA the irregular gaps in *k*-space result in the need for geometry-specific GRAPPA weights,[51,52] requiring large amounts of calibration data. These drawbacks often restrict the use of non-Cartesian parallel imaging to applications where real-time visualization is not necessary. One exception is through-time GRAPPA, where multiple fully sampled non-Cartesian datasets are acquired and are used to learn the location-specific GRAPPA weights.[53–55]

The level of acceleration achievable using parallel imaging is, in theory, equal to the number of independent coil elements along the direction of undersampling. In practice, acceleration rates are often limited to 2–3 using Cartesian trajectories, and 3–4 using non-Cartesian trajectories. Higher levels of acceleration can be achieved by combining temporal and spatial encoding schemes. These techniques often leverage the fact that the MR data are sparse in $\vec{x}$-f space, including; $\vec{k}$-t broad-use linear acquisition speed-up technique (BLAST), $\vec{k}$-t SENSE, $\vec{k}$-t GRAPPA.[56] In these schemes, the reconstruction is constrained using some prior information that can be used to determine the ground truth. These techniques often preclude real-time reconstruction, as this prior information is extracted from the data itself,[57] or as part of a prescan.

Even higher acceleration factors are possible using constrained reconstructions,[58] compressed sensing,[59] and regularized nonlinear inversion (NLINV).[60] These methods rely on object models, such as sparsity in a known transform domain, along with data sampling that produces incoherent aliasing in the sparsity domain. Some of the most popular sparsifying transforms for RT-MRI are finite differences, total variation, wavelet, and Fourier transform, which can be applied to exploit spatial and/or temporal sparsity. This category of methods enables acquisition of exceptionally high temporal and/or spatial resolution; however, they rely on nonlinear reconstruction that is computationally expensive, resulting in high reconstruction latency that often limits clinical adoption.

There has been substantial work towards reducing image reconstruction times. This includes the use of coil selection[61] and coil compression[62] techniques. Modern graphics processing units (GPUs) enable improvements in latency and throughput, through their massively parallel architecture,[63–65] and have enabled up to 27-fold reduction in latency compared to conventional CPUs,[66] making interactive RT-MRI feasible.

In addition, the efficient *k*-space trajectories often used in RT-MRI are susceptible to artifacts from linear time-invariant gradient distortions, including eddy currents. Correction of these has been shown to be feasible in real time.[23] However, artifacts from concomitant fields[67,68] are more challenging. At present, these require the use of approximations,[69] or the use of NMR field probes,[70,71] in conjunction with a more sophisticated offline reconstruction.[72]

Vendor-agnostic raw data formats have been developed to promote reconstruction algorithm sharing and data sharing, for example ISMRM Raw Data (ISMRMRD)[73] and Raw Array (RA).[74] The ISMRMRD format is designed to support simultaneous streaming of raw data, pulse sequence waveforms, and physiology waveforms, to image reconstruction or processing software.[75] This streaming capability is important for fast reconstruction of real-time images.

Postprocessing

Offline processing, including segmentation, parameter quantification, and distortion correction, of RT-MRI images is quite similar to traditional offline processing of CINE imaging or

even static imaging. However, there are many scenarios where inline postprocessing adds value, particularly for interactive RT-MRI. The unique features of these methods in RT-MRI are that they typically have to tolerate lower image SNR and have to satisfy maximum latency requirements. Inline segmentation has been shown to aid monitoring of ventricular function during cardiac interventions.[76] Inline flow quantification has been shown to expedite comprehensive cardiac examinations.[77] And inline off-resonance artifact correction (deblurring) has been shown to substantially improve the sharpness of speech articulator depiction.[78]

Interaction/Visualization

RT-MRI applications often benefit from the synchronization with other complementary real-time inputs. For cardiopulmonary testing, physiological monitoring of ECG, respiration, and expiratory gases may be synchronized with real-time cardiovascular imaging.[76] MRI-guided catheterization requires electrophysiological recording of high-fidelity ECG waveforms, which can be challenging within the MRI environment, and hemodynamic recording of invasive pressure waveforms.[79,80] Real-time speech imaging requires synchronization of audio signals with imaging data, which can be achieved with commercial products (eg, FORMI II+, Optoacoustics, Israel).[24,81]

Additionally, for some applications user interaction is required to modify parameters during imaging using real-time feedback to the scanner. Most notably, for real-time MRI-guided intervention the modification of slice position, slice thickness, slice orientation, image contrast, frame rate, and device imaging modules can each be toggled and modified interactively without a pause in the continuous stream of real-time imaging. Interactivity requires that images are displayed and manipulated in real-time, and that pulse sequence parameters are accessible to be modified on-the-fly.

Major MRI vendors have prototype or product graphical user interfaces for interactive imaging (eg, Monte Carlo prototype, Siemens Healthcare, Erlangen Germany; iSuite, Philips, Best, The Netherlands; iDrive and MR Echo, GE Healthcare, Waukesha, WI). Interactive imaging platforms are also available through independent MRI software vendors, most notably the RTHawk platform (Heart Vista, Los Altos, CA).[82] This platform is MRI vendor agnostic as long as a fully flexible stub sequence is available, but to date has been primarily developed on the GE platform. This system is compatible with interactive scan plane modification using a six degree-of-freedom 3D mouse.[82]

Auxiliary equipment can also be used inside of the MRI suite for interactive modification of imaging. MRI-guided catheterization procedures use foot-pedals to leave interventionist hands available for device manipulation, which mimics traditional x-ray catheterization suites. Other auxiliary equipment including computer mice, keyboards, and tablets have been explored for interactive imaging,[83] as well as gesture-based scan control.[84] Furthermore, augmented reality and virtual reality equipment[85] may be attractive for interactive visualization of real-time imaging in the future.

Applications

RT-MRI benefits a broad range of diagnostic and interventional applications. Here we summarize the application-specific needs, imaging considerations, and the impact to date.

Cardiac

RT-MRI enables imaging of the cardiovascular system without the need for cardiac gating or respiratory compensation. This is particularly valuable in patients with cardiac arrhythmia[86,87] where cardiac gating fails (~10% of patients referred for diagnostic cardiac imaging), and in patients who find breath-holding difficult (~10% of patients). It is also extremely valuable in children with congenital heart disease (CHD), where it can be used to lessen the need for sedation[88] and its associated risks.

Real-time assessment of cardiovascular structures requires relatively high spatial and temporal resolution to ensure accurate visualization and quantification. For example, Setser et al[89] recommend a minimum temporal resolution of 50 msec (20 fps), and spatial resolution of 2 mm for functional RT-MRI of the left ventricle. Real-time ventricular function imaging has been shown to achieve an excellent agreement with reference standard breath-held, cardiac gated techniques, through a combination of undersampled radial trajectories with $\vec{k}$-t SENSE reconstructions in CHD,[90] $\vec{k}$-t SPARSE-SENSE in patients with tachycardia[21] and myocardial infarction,[91] regularized nonlinear inversion,[92] and more recently, proof-of-concept studies using machine-learning reconstructions in CHD.[93] Figure 4a and Movie S1 contain a representative example of image quality. Spiral trajectories, although less popular, have been combined with compressed sensing to achieve high-resolution imaging in children with CHD.[96]

Quantification of blood flow using phase contrast (PC) requires high spatial resolution to mitigate partial volume effects; Greil et al recommend that it is necessary to have 16 pixels in the cross-section of the vessel of interest to get accurate flow quantification.[97] PC RT-MRI has been used clinically to assess the respiratory and cardiac components of flow in patients with Fontan circulation,[98,99] to quantify flow in children with cardiac left-to-right shunts,[100] to investigate the effect of elevated intrathoracic pressure on blood flow,[101] and in CHD.[94] Figure 4b and Movie S2 contain a representative example of image quality.

RT-MRI also enables imaging during exercise, which can be used to unmask subtle changes in early cardiovascular

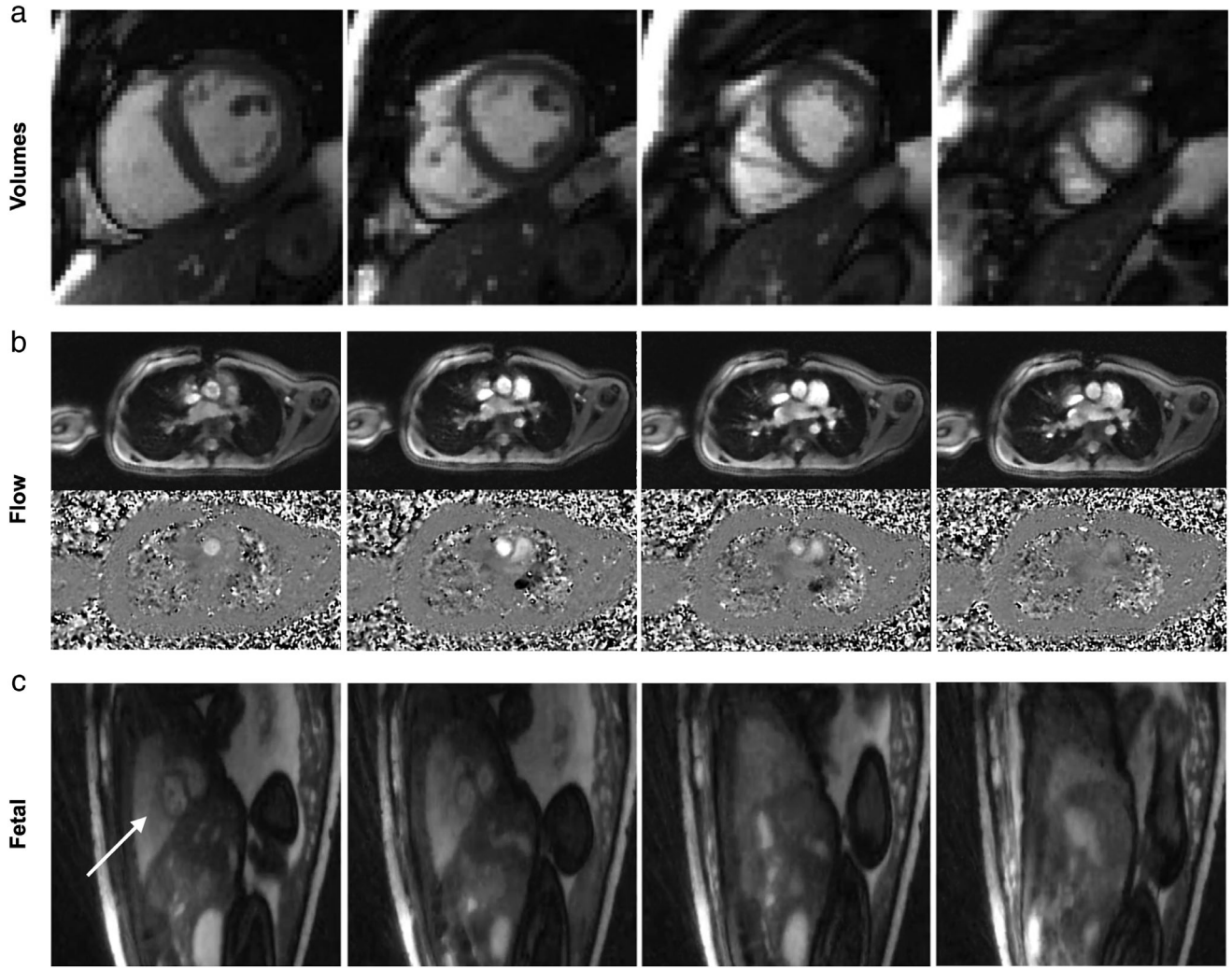

FIGURE 4: Illustration of cardiovascular RT-MRI. (a) Real-time cine imaging using tiny-golden angle radial bSSFP sequence at 1.5T, with 12x undersampling and compressive sensing reconstruction (TE/TR = 1.3/2.7 msec, flip angle = 70°, in-plane resolution = 2.1 mm, 32 msec temporal resolution, 31 fps). A movie can be found in Movie S1 [Adapted from Ref. (91)]. (b) Real-time PCMR using perturbed spirals at 1.5T, with 18x undersampling and compressive sensing reconstruction. Top: Magnitude images, Bottom: Phase images (TE/TR = 1.9/6.7 msec, VENC = 200 cm/s, flip angle = 20°, in-plane resolution = 1.8 mm, 27 msec temporal resolution, 37 fps). A movie can be found in Movie S2 [Adapted from Ref. (94)]. (c) Real-time imaging of the fetal heart (shown by arrow in first column) demonstrating gross fetal movement. Golden-angle radial bSSFP sequence at 1.5T, with 27x undersampling and compressive sensing reconstruction (TR = 5.0 msec, flip angle = 70°, in-plane resolution = 1.0 mm, 74 msec temporal resolution, 14 fps). A movie can be found in Movie S3 [Adapted from Ref. (95)].

disease.[102] Studies have shown the ability to measure ventricular volumes during exercise; to assess the effect of percutaneous pulmonary valve implantation,[103] to assess the mechanisms which augment cardiac output with exercise in repaired tetralogy of Fallot,[104] and to unmask right ventricular dysfunction in pulmonary arterial hypertension.[105] Real-time flow during exercise has also been used in patients with total cavopulmonary connection[106] and after surgical bypass of aortic arch obstruction.[107] Continuous acquisition of real-time flow during ramped exercise over 10 minutes has been shown,[63] as well as a combination with respiratory gas analysis to simultaneously measure peak oxygen consumption (VO_2), enabling assessment of exercise capacity.[108]

Fetal cardiac RT-MRI is of interest as a potential secondary tool (after fetal echocardiography) to characterize congenital cardiac malformations.[109] It is one of the most challenging applications of RT-MRI because of the very high heart rates, need for high spatial resolution (tiny hearts), need for interaction (to follow movement of the fetus), and the desire to be conservative with specific absorption rate (SAR) and acoustic noise.[110] It has been attempted with some success[95]; however, RT-MRI acquisition with retrospective metric-optimized-gating has provided a promising approach for CINE MRI. Figure 4c and Movie S3 contain a representative example of image quality of RT-MRI in the fetal heart.

MRI-Guided Invasive Procedures

MRI-guidance of diagnostic and therapeutic invasive procedures employ intraprocedural imaging to navigate devices and to assess procedural outcomes. Compared to traditional image-guidance modalities such as x-ray and ultrasound, MRI offers flexible image contrast and 3D imaging capabilities that can improve tissue visualization during a procedure. Real-time MRI is particularly valuable during complex device maneuvers and previous review articles have described the applications of real-time imaging technologies to guide invasive procedures.[111–113] Figure 5 and Movies S4 and S5 contain illustrative examples.

Many invasive procedures have been performed in patients in the MRI environment, including MRI-guided biopsy[117,118]; radiotherapy[119]; thermal ablations such as radiofrequency ablation,[120,121] laser ablation, cryoablation,[122] microwave ablation, and high-intensity focused ultrasound[123]; chemoablation; drug injection; electrophysiology[114,124,125]; and invasive pressure measurements.[80,115,126]

MRI-guided invasive procedures have unique requirements. Low-latency reconstruction and in-room image display are essential, such that images can be used for real-time device navigation and procedural decision-making. Interactivity of imaging parameters is critical to control image contrast and frame rate throughout the procedure. Image processing, including image segmentation, registration, and distortion correction, must also be performed on-the-fly.[112] During many invasive procedures, devices (eg, needles, catheters, guidewires, sheaths) are imaged concurrently with target anatomy. Device imaging is performed using either "passive" visualization, exploiting the material properties, or "active" visualization, in which devices themselves are RF receivers, designed as loopless antennas for imaging[127] or microcoils for 3D device tracking[128] (Fig. 5a, Movie S4). Solenoid and loopless receiver coils positioned on invasive devices can also be applied for small-FOV local imaging in MRI-endoscopy applications.[129]

Most in-bore biopsy procedures of prostate, liver, breast, and brain lesions use standard T_2-weighted, T_1-weighted, diffusion-weighted, or dynamic contrast-enhanced imaging for iterative confirmation of needle placement,[117,118,130] with a few studies employing high frame-rate dynamic needle guidance.[131,132] MRI-guided cardiovascular procedures are the most technically demanding, requiring rapid multiplanar imaging for device navigation. Most commonly, a 2D Cartesian bSSFP acquisition is used, in combination with parallel imaging, to achieve 5–10 frames/sec, with magnetization preparation pulses for contrast variation (Fig. 5b, Movie S5). 2D radial and spiral spoiled gradient echo acquisitions have also been applied for cardiovascular procedures,[133,134] and when combined with regularized nonlinear inversion reconstruction, have achieved a temporal resolution of 42 msec (24 fps) with reconstruction delay of 27 msec.[135]

RT-MRI thermometry, using proton resonance frequency shift imaging, is important to monitor thermal ablations with high temporal resolution. Multislice single-shot EPI acquisitions with real-time image registration methods have been developed for thermometry and dosimetry during cardiac RF ablations[116,136] (Fig. 5c, Movie S6). The geometry of transcranial high-intensity focused ultrasound (HIFU) therapy devices restrict the number of receive coils that can be positioned around the head, and undersampled stack-of-spiral and stack-of-stars EPI thermometry acquisitions[40,43] have been developed for volumetric brain coverage with 75-msec temporal resolution (13 fps). 3D dynamic keyhole imaging has generated high spatiotemporal resolution ($1.5\times1.5\times6$ mm^3 with 455 msec temporal resolution, 2 fps) imaging for dynamic guidance of radiotherapy.[137] This work utilizes a super-resolution generative model for high spatial reconstruction from low-spatial and high-temporal resolution images.

The unique set of requirements of MRI-guided invasive procedures continues to motivate the innovation of RT-MRI acquisitions, as well as rapid inline image reconstruction and image processing.

Upper Airway

RT-MRI enables imaging soft-tissue structures and muscles of the upper airway that are coordinated in space and time to perform essential human functions such as speech, respiration, and digestion. RT-MRI is preferred over other imaging and movement-tracking modalities because it allows for observing deep soft tissues such as the velum, pharyngeal wall, and the larynx in the arbitrary imaging plane without radiation or endoscopy. The nature of the movements of the upper airway is not necessarily periodic and is unrepeatable. RT-MRI can now be combined with intermittent tagging pulses to visualize internal deformation in the tongue muscles[138,139] and be exploited to reconstruct 3D tongue shape or model.[140,141] Real-time visualization and interaction are also advantageous for the operator to modify imaging parameters on-the-fly and to ensure subject compliance with stimuli.

Figure 6 and Movies S7–S9 illustrate representative research areas in speech production,[24,144] sleep apnea,[36,37,145] and swallowing.[60] Imaging is often performed along with synchronized recordings of physiological signals such as audio signals in speech,[146] polysomnography signals used in sleep studies,[36] and intraoral pressure sensor used in swallowing[143] to aid real-time or retrospective analysis. Several clinical applications have also been explored such as velopharyngeal insufficiency,[147] apraxia,[60,148] and postsurgical assessment of glossectomy[148,149] and cleft-palate repair.[150,151] Many other applications and technical aspects of the upper airway imaging have been described in review articles with focuses on speech,[24,144,152] speech and sleep,[153] sleep,[145] and image analysis techniques on RT-MRI of vocal tract motion.[154]

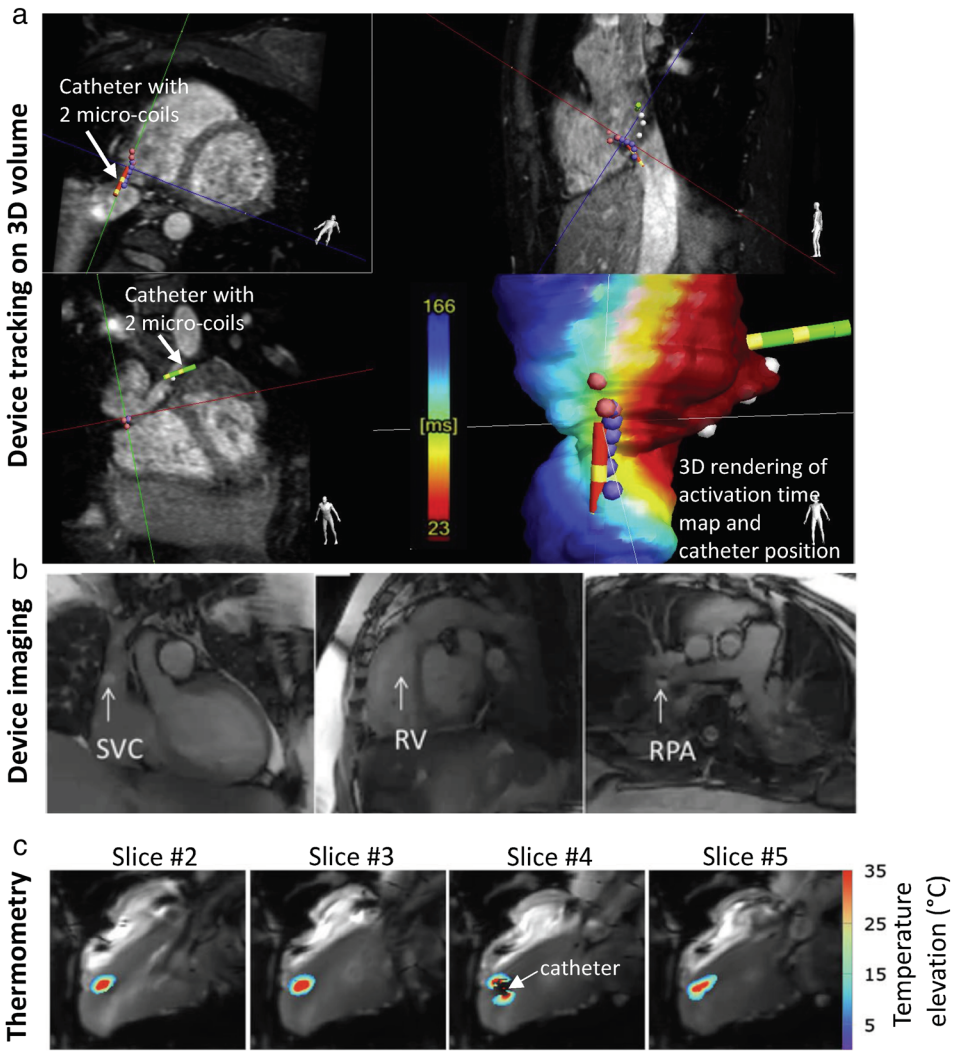

FIGURE 5: Illustrations of RT-MRI for MRI-guided invasive procedures. Cardiovascular procedures are the most technically demanding for RT-MRI, and therefore are provided. (a) The position and orientation of catheter devices with two embedded microcoils are tracked on a previously acquired 3D volume for an electrophysiology procedure. Real-time device tracing is achieved using 3D gradient echo projection imaging (resolution 0.83 mm, 10 Hz tracking rate) [Reproduced from Ref. (114)]. (b) Interactive RT-MRI used to navigate gadolinium-filled balloon wedge end-hole catheter during diagnostic right heart catheterization (bSSFP, TE/TR = 1.44/2.88 msec, flip angle = 40°, in-plane resolution = 1.8×2.4 mm^2, GRAPPA rate 2, 200 msec temporal resolution, 5 fps) [Adapted from Ref. (115)]. (c) Real-time MRI thermometry used to calculate thermal dose during therapeutic ablation procedure (gradient echo EPI, TE/TR = 18–20/110 msec, flip angle = 60°, in-plane resolution = 1.6×1.6 mm^2, GRAPPA rate 2, 200 msec temporal resolution, 5 slices/s) [Adapted from Ref. (116)].

The upper airway imaging generally requires high spatial and temporal resolution, although specific imaging parameters would be dictated by the applications shown in Fig. 1 in Lingala et al.[24] For speech, high temporal resolution, below 70 msec (greater than 14 fps) and spatial resolution of no more than 3.5 mm^2 are typically required to study a broad range of speech events. For sleep, pharyngeal airway motion is relatively slower than vocal tract motion, as it involves closure of the airway, requiring lower temporal resolution than imaging for speech and swallowing. For swallowing, it is valuable to track both the pharyngolaryngeal area and the lower esophageal sphincter and its surrounding area.[155]

Current state-of-the-art techniques use non-Cartesian sampling (radial or spiral acquisition) and parallel imaging, combined with constrained reconstruction. This has enabled 2D dynamic images with spatial resolutions of 1.3–2.4 mm^2 at high temporal resolutions of 10–60 msec (100 to 17 fps) from highly undersampled MRI data.[11,54,55,143,156–159] Imaging the 2D mid-sagittal plane is the most widely used, as it is most informative thanks to its entire vocal tract coverage from the lips to the glottis given a high temporal resolution. Imaging a few 2D planes,[11,29,30] simultaneous 2D planes,[36,37] or 3D[38] at the cost of temporal resolution have also been developed. Recently, 3D stack-of-spiral acquisition demonstrated imaging of the full vocal tract (FOV: 200×200×70 mm^3) with high spatiotemporal resolution (2.4×2.4×5.8 mm^3, with 72 msec temporal resolution, 14 fps) during natural speech.[39]

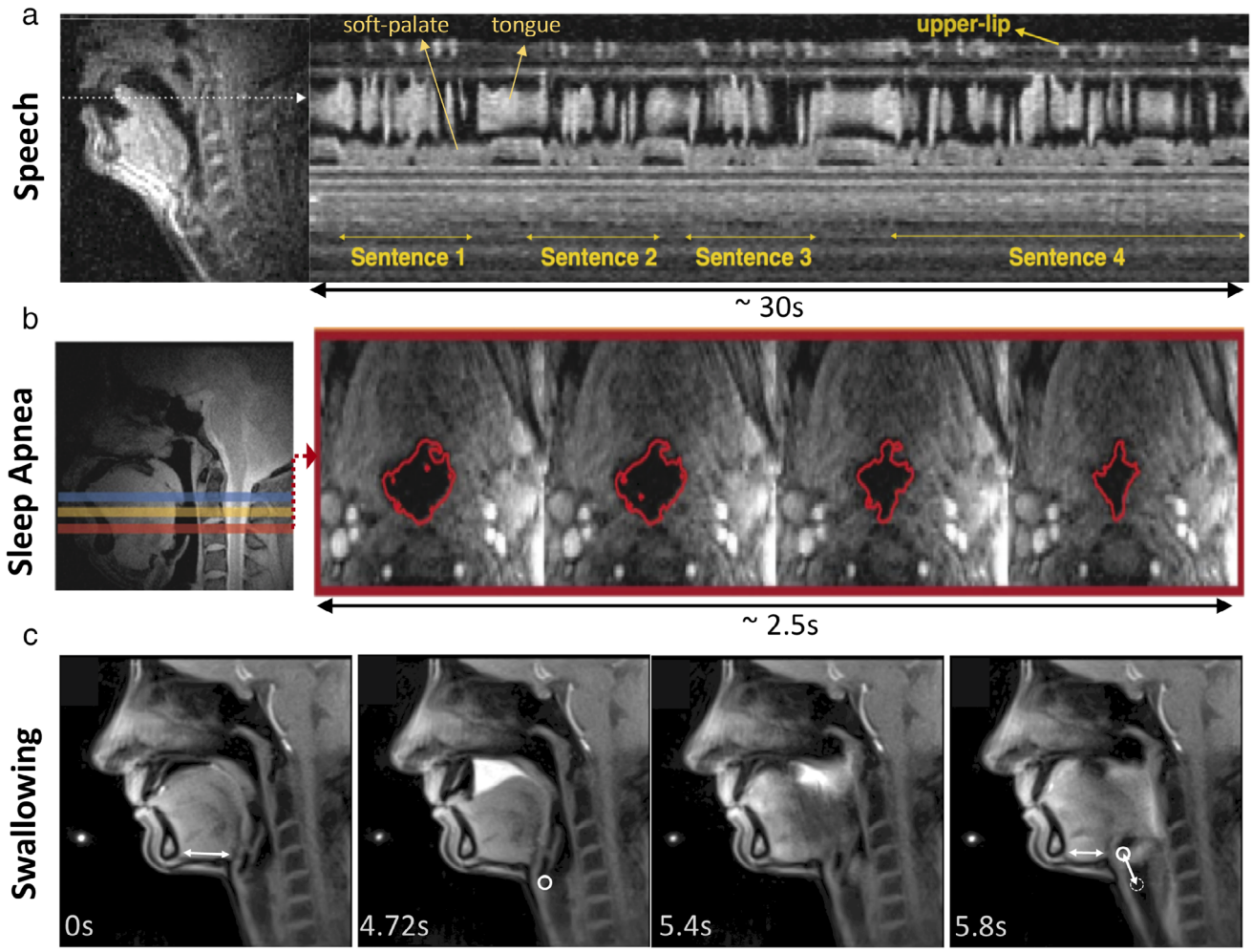

FIGURE 6: Illustration of upper airway RT-MRI. (a) Speech production imaging using 13-interleave spiral GRE sequence at 1.5T (TE/TR = 0.8/6.0 msec, flip angle = 15°, in-plane resolution = 2.4 mm, 12 msec temporal resolution, 83 fps) [Adapted from Ref. (142)]. (b) Sleep apnea study using simultaneous multislice radial GRE sequence at 3T (TE/TR = 3.7/6.5 msec, flip angle = 5°, slice thickness/gap = 7/3 mm, 3 slices, in-plane resolution = 1 mm, 96 msec temporal resolution, 10 fps) [Adapted from Ref. (37)]. (c) Swallowing imaging of 10-ml pineapple juice using radial FLASH sequence (TE/TR = 1.33/2.10 msec, flip angle = 8°, in-plane resolution = 1.3 mm, 40 msec temporal resolution, 25 fps, 19 spokes) [Adapted from Ref. (143)].

Imaging the upper airway has a unique challenge: tissue surfaces along the upper airway are the main region of interest but are vulnerable to off-resonance effects. Those include the movements of the articulators during speech or swallowing, the closure of the velopharyngeal port in velopharyngeal insufficiency, and the collapse of the pharyngeal airway in sleep studies. Off-resonance at the tissue surfaces manifest as blurring or signal loss with non-Cartesian sampling such as spirals and/or appear as banding artifact when bSSFP sequences are used. Careful shimming is usually carried out with a focus on the tissue boundaries. Current RT-MRI studies for speech production are most often conducted using short-duration spirals (2.5 msec) and/or at lower field strength (1.5T or lower) MRI scanners, or in conjunction with field inhomogeneity reconstruction[160–162] or, more recently, artificial intelligence (AI)-based deblurring.[78]

Musculoskeletal

Musculoskeletal RT-MRI is used to reveal abnormal joint biomechanics, which are linked to joint disorders, usually in the context of pain, instability, or movement restriction. For example, abnormal knee kinematics is known to contribute to the development and progression of osteoarthritis. Common musculoskeletal applications include the knee, wrist, spine, temporomandibular joint, foot, and hip,[163] with a selected few illustrated in Fig. 7 and Movies S10–S12. These have vastly different spatiotemporal resolution and coverage needs.

Early work used semi-static approaches (multiple static images in fixed postures). Systematic studies have since determined that biomechanical models derived from RT-MRI are substantially different from those derived from semi-static approaches,[167] making RT-MRI the current method of choice. Musculoskeletal movements are voluntary, and can

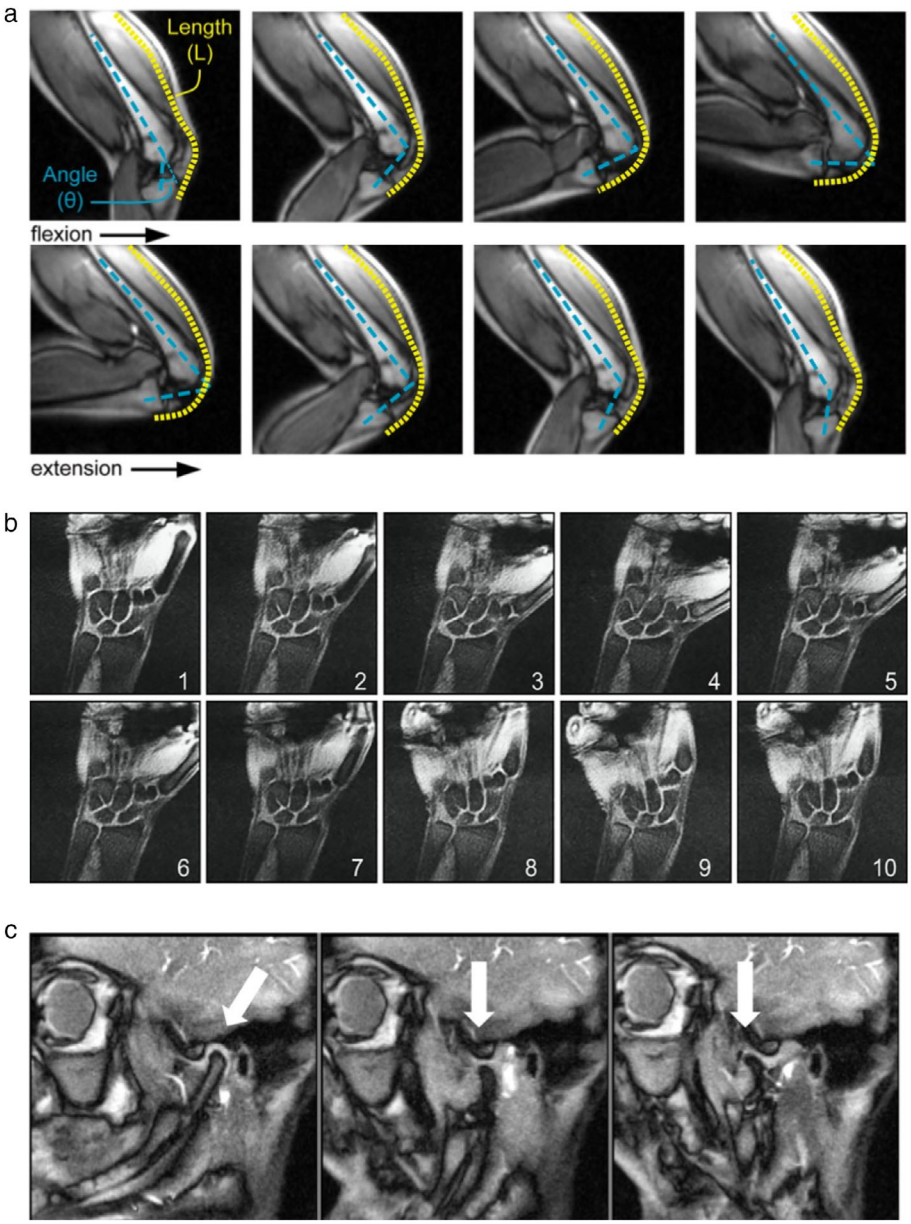

FIGURE 7: Illustration of three musculoskeletal RT-MRI applications. (a) Knee RT-MRI highlighting flexion, extension, and the measurement of rectus femoris knee muscle moment arms [Adapted from Ref. (164)]. (b) Wrist RT-MRI illustrating a radial–ulnar deviation maneuver, suitable for measuring dynamics of the scapholunate gap [Adapted from Ref. (165)]. (c) Temporomandibular joint RT-MRI illustrating the ability to track condyle movement during voluntary opening of the mouth [Adapted from Ref. (166)].

sometimes be performed through controlled dynamics, for example where movements are repeated and synchronized with a metronome or periodic visual stimulus. However, voluntary synchronization is imprecise, subject-dependent, and impractical for patients with pain. Retrospective gating can be applied using additional sensors[168] or self-gating approaches,[169] assuming that the timing variations have a negligible impact on kinematic estimates. Movement can be more precisely controlled by a physical apparatus, but this does not lead to realistic physical effort, which is often needed to reproduce the abnormal movement and/or the symptom being studied (eg, pain). Finally, it is possible to synchronize using external muscle stimulation,[170] which adds experimental complexity. For all of these reasons, there is a need for RT-MRI, and often a need for an appropriate load.[171]

Musculoskeletal RT-MRI requires strong contrast between muscle, fat, and surrounding fluids, and benefits from high SNR efficiency, making bSSFP the sequence of choice.[172] bSSFP can be augmented with phase-sensitive reconstruction for fat–water separation.[173] GRE may also be used with optional multiecho fat–water separation.[174] Most studies in the literature were performed at conventional field strengths (1.5T and 3T) in the supine position, which restricts movement and load bearing. For this reason, low-field

open-bore, and upright MRI has been explored as an alternative to alleviate these restrictions.[175]

In the knee, RT-MRI has provided valuable insight into patellofemoral pain, and used to quantify kinematics,[176] document the differences between the load-bearing and nonload-bearing kinematics,[177] and determine the effects of physical supports.[176] RT-MRI measurement of tibiofemoral kinematics can be further improved by using slice-to-volume registration with 3D static scans.[178,179] In the finger, 2D RT-MRI has provided insight into joint cavitation, which is responsible for the cracking sound.[180] In the wrist, 2D and 3D RT-MRI have provided insight into ligament insufficiency, instability, and how aberrant kinematics may contribute to wrist pain.[165,181] In the shoulder, low-resolution RT-MRI in conjunction with high-resolution static MRI was used to better characterize rotator cuff disease.[182] In the temporomandibular joint, RT-MRI has been demonstrated with adequate spatiotemporal resolution to track disc and condyle kinematics.[166,183] In summary, RT-MRI is a promising early-stage technique for studying musculoskeletal kinematic insufficiency/abnormality and pain in several body regions.

Other

RT-MRI has also been used for other thorax and abdominal imaging applications. Real-time cine imaging has been used to assess abnormal bowel motility following ingestion of an oral contrast agent (eg, mannitol). Bowel imaging is typically performed in a coronal orientation and bSSFP imaging has been applied for imaging for 1–3 seconds temporal resolution per 3D volume (1 to 0.3 fps).[184,185] Dynamic esophageal imaging has been achieved using a radial spoiled gradient echo acquisition with nonlinear inverse image reconstruction for 40-msec temporal resolution (25 fps) following the ingestion of pineapple juice.[186] RT-MRI has also been used in urethrography, to assess urinary function during bladder emptying,[187] in defecography, to assess the pelvic floor in mechanical and functional rectal disorders,[188] and to asses pelvic floor disorder and pelvic organ prolapse.[189] These techniques often use turbo-spin-echo sequences to achieve T_2 weighting, with 1.0–1.5 mm spatial resolution, and a temporal resolution of 1–5 seconds (1 to 0.2 fps).

RT-MRI has also proven valuable for screening of fetal central nervous system abnormalities, specifically the structural malformations.[190–192] T_2-weighted RARE sequences (often with partial echo along the phase-encode direction) are used for beneficial contrast between gray and white matter.

This article focused on the use of RT-MRI in imaging physical motion; however, it can also be used to image contrast dynamics. Although this is beyond the scope of this article, this includes dynamic contrast-enhanced MRI,[193] time-resolved angiography,[194] as well as functional MRI,[42] including arterial spin labeling (ASL)[195] and encephalography.[196]

Current Directions

Increasing Role of ML/AI

In recent years, machine-learning (ML) methods, especially deep learning, have enabled breakthroughs in computer vision and image analysis. The astonishing success of deep-learning algorithms has penetrated areas of MR image reconstruction, artifact correction, automatic classification and segmentation, landmark detection, and so on.

Deep learning has huge potential in RT-MRI applications; for example, in real-time visualization and/or immediate downstream analysis. There have been several early works on ML with success for RT-MRI applications, as illustrated in Fig. 8 and Movies S13 and S14. This figure demonstrates the use of deep learning for various tasks; reconstruction of RT-MRI data (removing artifact from undersampled radial images, Fig. 8a), improving image quality of RT-MRI (performing off-resonance deblurring, Fig. 8b), and to enhance clinical impact (performing needle detection and segmentation, Fig. 8c). It has been shown to be popular for low-latency reconstructions of real-time MR data; in 2D cardiac imaging,[93,198,199] MR-guided radiotherapy images,[200] and 3D functional MRI.[201] Additionally, it is popular for rapid postprocessing of real-time data; including identification and segmentation of the vocal tract,[202–205] as well as segmentation of the left and right ventricles from real-time cardiac MRI.[206] Other applications include rapid needle detection and segmentation in MR-guided interventions,[197,207] enabling real-time localization of the fetal brain,[208] spiral off-resonance deblurring in speech imaging,[78] and a combination of reconstruction and postprocessing for real-time MR thermometry.[209]

Some commercially available software has started using ML in real-time imaging, including HeartVista,[210] which uses ML to automate the MRI exam, control the scanner and assist scan planning, and MeVisLab[211] for segmentation and annotation.

High-Performance Low Field

Recent publications have suggested substantial opportunities for real-time imaging on high-performance low field (HPLF) MRI systems.[212] These systems operate with a low static field strength (eg, 0.35T and 0.55T) and incorporate contemporary high-performance hardware and modern imaging methods. Unlike historic low-field MRI systems, these HPLF systems include fast shielded gradients and multichannel receiver arrays. They are capable of non-Cartesian sampling, parallel imaging, and compressed sensing, and can exploit readily available computational resources. These systems have produced new capability and exceptional performance for cardiac, abdominal, and pulmonary RT-MRI, illustrated in Fig. 9 and Movie S15.

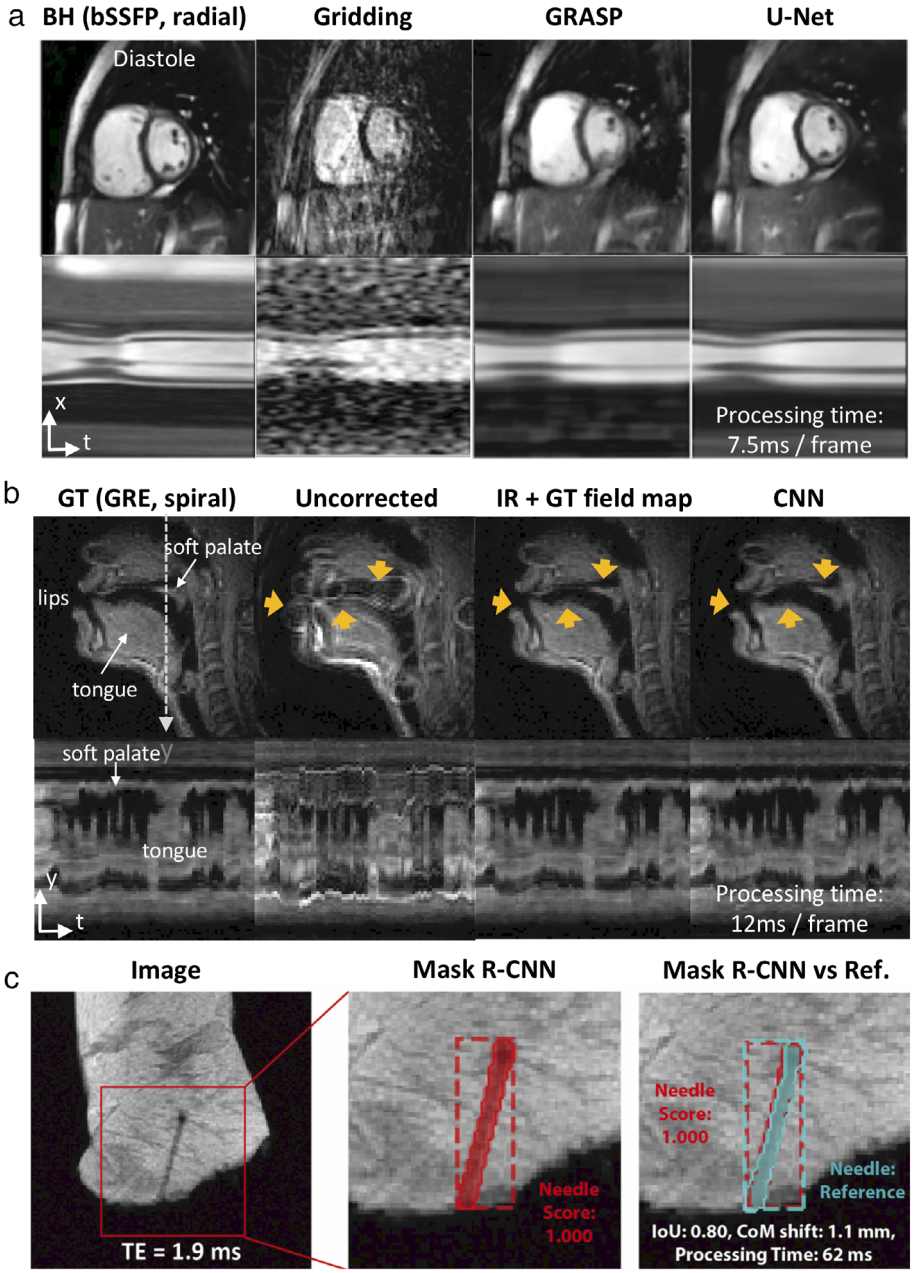

FIGURE 8: Illustration of three ML/AI-based low-latency applications. (a) Image reconstruction of cardiovascular imaging; (left-to-right) the BH-bSSFP sequence and the RT radial sequence reconstructed with gridding, GRASP, and the residual U-Net [Adapted from Ref. (93)] (b) Spiral off-resonance deblurring of speech imaging; (left-to-right) GT, uncorrected, IR with GT field map, and the CNN [Adapted from Ref. (78)]. (C) Needle detection and segmentation for ex vivo tissue RT-MRI; (left-to-right) Original image, needle detection and segmentation result using Mask R-CNN, result comparison against a reference [Adapted from Ref. (197)]. Note that "processing time" shown here is the time to run the neural networks and does not include the time to do preprocessing of the data. BH: breath-hold, GRASP: Golden-angle radial sparse parallel imaging, PT: processing time, GT: ground truth, IR: iterative reconstruction.

The HPLF system configuration provides several advantages for real-time imaging. 1) Many RT-MRI acquisitions are limited by off-resonance (eg, bSSFP, spiral). Since absolute off-resonance (in Hz) scales linearly with field strength, lower field strength systems relax this constraint. For bSSFP acquisitions, longer TRs can be used without banding artifacts. For spiral sampling, longer readouts can be used without blurring artifacts. 2) T_2* is longer, making it possible for efficient data-sampling strategies, including spiral and EPI and to be implemented with prolonged duration. This allows increased flexibility in trajectory design. Moreover, artifacts related to susceptibility (eg, blurring and ghosting) are reduced. 3) T_1 is shorter at lower field strength, causing more rapid signal recovery between RF pulses. 4) Tissue heating due to RF is reduced at low field, which permits high flip angle excitation and magnetization preparation pulses, with

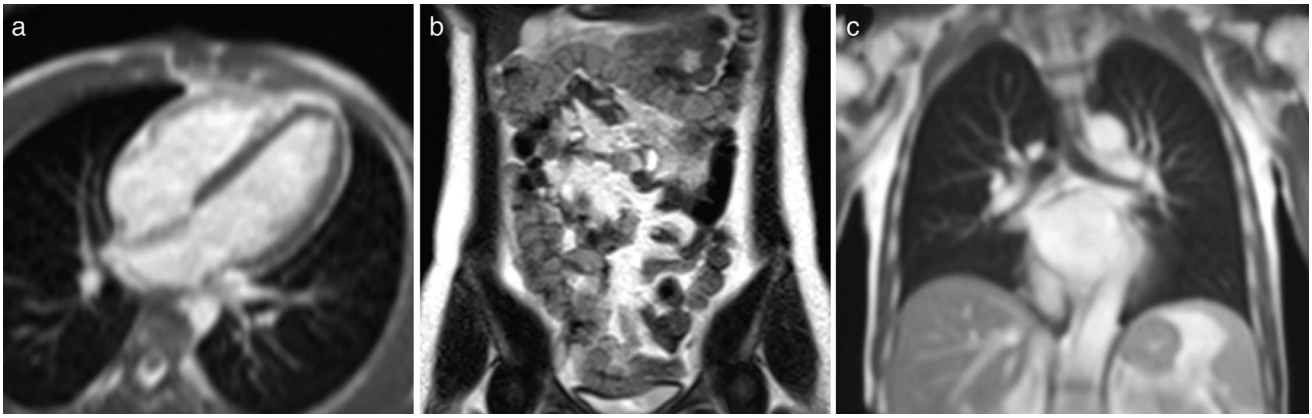

FIGURE 9: Demonstration of real-time bSSFP imaging using a high-performance low field (HPLF) MRI system (prototype 0.55T Aera, Siemens Healthcare, Erlangen, Germany). (a) Real-time bSSFP for MRI-guided invasive cardiovascular procedures (TE/TR = 2.0/4.0 msec, flip angle = 45°, in-plane resolution = 2 mm, slice thickness = 8 mm, GRAPPA rate 2, 250 msec temporal resolution, 4 fps). (b) Real-time bSSFP for dynamic intestinal imaging (TE/TR = 1.6/3.2 msec, flip angle = 90°, in-plane resolution = 1.2 mm, slice thickness = 10 mm, GRAPPA rate 3, 1.2 sec temporal resolution for 6 slices, 0.8 fps). No bSSFP banding around the intestines is observed using the HPLF system configuration. (c) Real-time bSSFP for dynamic respiratory imaging (TE/TR = 1.21/2.4 msec, flip angle = 70°, in-plane resolution = 1.8 mm, slice-thickness = 15 mm, GRAPPA rate 2, 250 msec temporal resolution, 4 fps). Due to the reduced susceptibility, higher-quality imaging of lung parenchyma is feasible.

diminishing concerns of patient safety during prolonged real-time imaging. The net result is a favorable system configuration for real-time imaging.

HPLF is especially beneficial for MR-guided interventions, due to the favorable low SAR properties. Reduced device heating will enable the application of commercial conductive devices in the MRI environment, and reduce the burden of design for new devices, which is substantial at conventional field strengths (≥1.5T).[213] HPLF is also beneficial for real-time speech imaging, where susceptibility gradients at air–tissue interfaces are the primary constraint.

Finally, an HPLF system could be cost-effective to manufacture, install, and maintain, which may increase accessibility for these real-time imaging applications outside of the conventional radiology environment (eg, cardiology and point-of-care settings). Currently, the B_0 subsystem comprises roughly 30% of system cost.[214] Therefore, a reduction in field strength and potential complexity (ie, simplified cooling and maintenance) could enable an attractive value system.

Concluding Remarks

MRI has historically been applied to static imaging of the brain, spine, and joints, due to its relatively slow speed. Leaps in MRI technology and information extraction over the last two decades have made it possible to image more broadly, including areas of the body that experience substantial motion and even irregular motion, and including the real-time guidance of interventions. RT-MRI has a rich history and an even brighter future. It is a key enabling technology for MRI to penetrate new diagnostic and interventional applications.

Acknowledgments

A.C.W. acknowledges the assistance of Siemens Healthcare in the modification of the NHLBI MRI system for operation at 0.55T under an existing cooperative research agreement between NHLBI and Siemens Healthcare. This system was used to generate Fig. 9 and Movie S15.

References

1. Dietz B, Fallone BG, Wachowicz K. Nomenclature for real-time magnetic resonance imaging. Magn Reson Med 2019;81(3):1483-1484.
2. Nayak KS. Response to letter to the editor: "Nomenclature for real-time magnetic resonance imaging.". Magn Reson Med 2019;82(2):525-526.
3. Mansfield P. Multi-planar image formation using NMR spin echoes. J Phys C Solid State Phys 1977;10:L55-L58.
4. Frahm J, Haase A, Matthaei D. Rapid NMR imaging of dynamic processes using the FLASH technique. Magn Reson Med 1986;3(2):321-327.
5. Hennig J, Nauerth A, Friedburg H. RARE imaging: A fast imaging method for clinical MR. Magn Reson Med 1986;3(6):823-833.
6. Farzaneh F, Riederer SJ, Lee JN, Tasciyan T, Wright RC, Spritzer CE. MR fluoroscopy: Initial clinical studies. Radiology 1989;171(2):545-549.
7. Holsinger AE, Wright RC, Riederer SJ, Farzaneh F, Grimm RC, Maier JK. Real-time interactive magnetic resonance imaging. Magn Reson Med 1990;14(3):547-553.
8. Riederer SJ, Wright RC, Ehman RL, et al. Real-time interactive color flow MR imaging. Radiology 1991;181(1):33-39.
9. Kerr AB, Pauly JM, Hu BS, et al. Real-time interactive MRI on a conventional scanner. Magn Reson Med 1997;38(3):355-367.
10. Macovski A. Noise in MRI. Magn Reson Med 1996;36(3):494-497.
11. Lingala SG, Zhu Y, Kim Y-C, Toutios A, Narayanan S, Nayak KS. A fast and flexible MRI system for the study of dynamic vocal tract shaping. Magn Reson Med 2017;77(1):112-125.

12. Kim YC, Hayes CE, Narayanan SS, Nayak KS. Novel 16-channel receive coil array for accelerated upper airway MRI at 3 Tesla. Magn Reson Med 2011;65(6):1711-1717.

13. Kim YC, Narayanan SS, Nayak KS. Flexible retrospective selection of temporal resolution in real-time speech MRI using a golden-ratio spiral view order. Magn Reson Med 2011;65(5):1365-1371.

14. Scheffler K, Lehnhardt S. Principles and applications of balanced SSFP techniques. Eur Radiol 2003;13(11):2409-2418.

15. Reeder SB, Markl M, Yu H, Hellinger JC, Herfkens RJ, Pelc NJ. Cardiac CINE imaging with IDEAL water-fat separation and steady-state free precession. J Magn Reson Imaging 2005;22(1):44-52.

16. Lustig M, Santos JM, Donoho DL, Pauly JM. k-t SPARSE: High frame rate dynamic MRI exploiting spatio-temporal sparsity. In: Proc 14th Annual Meeting ISMRM, Seattle; 2006. p 2420.

17. Feng L, Srichai MB, Lim RP, et al. Highly accelerated real-time cardiac cine MRI using k–t SPARSE-SENSE. Magn Reson Med 2013;70(1): 64-74.

18. Jung H, Sung K, Nayak KS, Kim EY, Ye JC. K-t FOCUSS: A general compressed sensing framework for high resolution dynamic MRI. Magn Reson Med 2009;61(1):103-116.

19. Otazo R, Kim D, Axel L, Sodickson DK. Combination of compressed sensing and parallel imaging for highly accelerated first-pass cardiac perfusion MRI. Magn Reson Med 2010;64(3):767-776.

20. Gamper U, Boesiger P, Kozerke S. Compressed sensing in dynamic MRI. Magn Reson Med 2008;373:365-373.

21. Bassett EC, Kholmovski EG, Wilson BD, et al. Evaluation of highly accelerated real-time cardiac cine MRI in tachycardia. NMR Biomed 2014;27(2):175-182.

22. Kim Y-C, Nielsen J-F, Nayak KS. Automatic correction of echo-planar imaging (EPI) ghosting artifacts in real-time interactive cardiac MRI using sensitivity encoding. J Magn Reson Imaging 2008;27(1): 239-245.

23. Campbell-Washburn AE, Xue H, Lederman RJ, Faranesh AZ, Hansen MS. Real-time distortion correction of spiral and echo planar images using the gradient system impulse response function. Magn Reson Med 2016;75(6):2278-2285.

24. Lingala SG, Sutton BP, Miquel ME, Nayak KS. Recommendations for real-time speech MRI. J Magn Reson Imaging 2016;43(1):28-44.

25. Winkelmann S, Schaeffter T, Koehler T, Eggers H, Doessel O. An optimal radial profile order based on the golden ratio for time-resolved MRI. IEEE Trans Med Imaging 2007;26(1):68-76.

26. Wundrak S, Paul J, Ulrici J, Hell E, Rasche V. A small surrogate for the golden angle in time-resolved radial MRI based on generalized Fibonacci sequences. IEEE Trans Med Imaging 2015;34(6):1262-1269.

27. Nayak KS, Pauly JM, Nishimura DG, Hu BS. Rapid ventricular assessment using real-time interactive multislice MRI. Magn Reson Med 2001;45(3):371-375.

28. Bornstedt A, Nagel E, Schalla S, Schnackenburg B, Klein C, Fleck E. Multi-slice dynamic imaging: Complete functional cardiac MR examination within 15 seconds. J Magn Reson Imaging 2001;14(3):300-305.

29. Kim YC, Proctor MI, Narayanan SS, Nayak KS. Improved imaging of lingual articulation using real-time multislice MRI. J Magn Reson Imaging 2012;35(4):943-948.

30. Feng X, Inouye JM, Blemker SS, et al. Assessment of velopharyngeal function with multi-planar high-resolution real-time spiral dynamic MRI. Magn Reson Med 2018;80:1467-1474.

31. Krohn S, Joseph AA, Voit D, et al. Multi-slice real-time MRI of temporomandibular joint dynamics. Dentomaxillofac Radiol 2018;48(1): 20180162.

32. Larkman DJ, Hajnal JV, Herlihy AH, Coutts GA, Young IR, Ehnholm G. Use of multicoil arrays for separation of signal from multiple slices simultaneously excited. J Magn Reson Imaging 2001;13(2):313-317.

33. Hamilton JI, Wright KL, Griswold MA, Seiberlich N. Self-calibrating interleaved reconstruction for through-time non-Cartesian GRAPPA. In: Proc 21st Annual Meeting ISMRM, Salt Lake City; 2013, p 3836.

34. Setsompop K, Gagoski BA, Polimeni JR, Witzel T, Wedeen VJ, Wald LL. Blipped-controlled aliasing in parallel imaging for simultaneous multislice echo planar imaging with reduced g-factor penalty. Magn Reson Med 2012;67(5):1210-1224.

35. Rosenzweig S, Holme HCM, Wilke RN, Voit D, Frahm J, Uecker M. Simultaneous multi-slice MRI using Cartesian and radial FLASH and regularized nonlinear inversion: SMS-NLINV. Magn Reson Med 2018; 79(4):2057-2066.

36. Wu Z, Chen W, Khoo MCK, Davidson Ward SL, Nayak KS. Evaluation of upper airway collapsibility using real-time MRI. J Magn Reson Imaging 2016;44(1):158-167.

37. Chen W, Gillett E, Khoo MCK, Davidson Ward SL, Nayak KS. Real-time multislice MRI during continuous positive airway pressure reveals upper airway response to pressure change. J Magn Reson Imaging 2017;46(5):1400-1408.

38. Burdumy M, Traser L, Burk F, et al. One-second MRI of a three-dimensional vocal tract to measure dynamic articulator modifications. J Magn Reson Imaging 2017;46(1):94-101.

39. Lim Y, Zhu Y, Lingala SG, Byrd D, Narayanan S, Nayak KS. 3D dynamic MRI of the vocal tract during natural speech. Magn Reson Med 2019;81:1511-1520.

40. Fielden SW, Feng X, Zhao L, et al. A spiral-based volumetric acquisition for MR temperature imaging. Magn Reson Med 2018;79(6):3122-3127.

41. Mansfield P, Howseman AM, Ordidge RJ. Volumar imaging using NMR spin echoes: Echo-volumar imaging (EVI) at 0.1 T. J Phys E 1989;22(5):324-330.

42. van der Zwaag W, Francis S, Bowtell R. Improved echo volumar imaging (EVI) for functional MRI. Magn Reson Med 2006;56(6):1320-1327.

43. Jonathan SV, Grissom WA. Volumetric MRI thermometry using a three-dimensional stack-of-stars echo-planar imaging pulse sequence. Magn Reson Med 2018;79(4):2003-2013.

44. Kim Y-C, Lebel RM, Wu Z, Ward SLD, Khoo MCK, Nayak KS. Real-time 3D magnetic resonance imaging of the pharyngeal airway in sleep apnea. Magn Reson Med 2014;71(4):1501-1510.

45. Sabati M, Lauzon ML, Nagarajappa N, Frayne R. A real-time 3D large field-of-view MRI system with interactive table motion. Concepts Magn Reson Part B Magn Reson Eng 2006;29B(1):28-41.

46. Riederer SJ, Tasciyan T, Farzaneh F, Lee JN, Wright RC, Herfkens RJ. MR fluoroscopy: Technical feasibility. Magn Reson Med 1988;8(1): 1-15.

47. Pruessmann KP, Weiger M, Scheidegger MB, Boesiger P. SENSE: Sensitivity encoding for fast MRI. Magn Reson Med 1999;42(5):952-962.

48. Griswold MA, Jakob PM, Heidemann RM, et al. Generalized autocalibrating partially parallel acquisitions (GRAPPA). Magn Reson Med 2002;47(6):1202-1210.

49. O'Sullivan JD. A fast sinc function gridding algorithm for Fourier inversion in computer tomography. IEEE Trans Med Imaging 1985;4(4): 200-207.

50. Pruessmann KP, Weiger M, Börnert P, Boesiger P. Advances in sensitivity encoding with arbitrary k-space trajectories. Magn Reson Med 2001;46(4):638-651.

51. Seiberlich N, Breuer FA, Blaimer M, Barkauskas K, Jakob PM, Griswold MA. Non-Cartesian data reconstruction using GRAPPA operator gridding (GROG). Magn Reson Med 2007;58(6):1257-1265.

52. Seiberlich N, Griswold M. Self-calibrating through-time spiral GRAPPA for real-time CMR. J Cardiovasc Magn Reson 2013;15(1):E28.

53. Seiberlich N, Ehses P, Duerk J, Gilkeson R, Griswold M. Improved radial GRAPPA calibration for real-time free-breathing cardiac imaging. Magn Reson Med 2011;65(2):492-505.

54. Lingala SG, Zhu Y, Lim Y, et al. Feasibility of through-time spiral generalized autocalibrating partial parallel acquisition for low latency accelerated real-time MRI of speech. Magn Reson Med 2017;78:2275-2282.

55. Ruthven M, Freitas AC, Boubertakh R, Miquel ME. Application of radial GRAPPA techniques to single- and multislice dynamic speech MRI using a 16-channel neurovascular coil. Magn Reson Med 2019;82 (3):948-958.

56. Huang F, Akao J, Vijayakumar S, Duensing GR, Limkeman M. k-t GRAPPA: A k-space implementation for dynamic MRI with high reduction factor. Magn Reson Med 2005;54(5):1172-1184.

57. Ponce IP, Blaimer M, Breuer FA, Griswold MA, Jakob PM, Kellman P. Auto-calibration approach for k–t SENSE. Magn Reson Med 2014;71 (3):1123-1129.

58. Liang Z-P, Boada F, Constable R, Haacke E, Lauterbur P, Smith M. Constrained reconstruction methods in MR imaging. Rev Magn Reson Med 1992;4:67-185.

59. Lustig M, Donoho DL, Santos JM, Pauly JM. Compressed sensing MRI. IEEE Signal Process Mag 2008;25(2):72-82.

60. Zu Y, Narayanan SS, Kim Y-C, et al. Evaluation of swallow function after tongue cancer treatment using real-time magnetic resonance imaging: A pilot study. JAMA Otolaryngol Head Neck Surg 2013;139 (12):1312-1319.

61. Müller S, Umathum R, Speier P, et al. Dynamic coil selection for real-time imaging in interventional MRI. Magn Reson Med 2006;56(5): 1156-1162.

62. Buehrer M, Pruessmann KP, Boesiger P, Kozerke S. Array compression for MRI with large coil arrays. Magn Reson Med 2007;57(6):1131-1139.

63. Kowalik GT, Steeden JA, Pandya B, et al. Real-time flow with fast GPU reconstruction for continuous assessment of cardiac output. J Magn Reson Imaging 2012;36(6):1477-1482.

64. Sorensen TS, Atkinson D, Schaeffter T, Hansen MS. Real-time reconstruction of sensitivity encoded radial magnetic resonance imaging using a graphics processing unit. IEEE Trans Med Imaging 2009;28 (12):1974-1985.

65. Schaetz S, Uecker M. A multi-GPU programming library for real-time applications. In: Proceedings of the 12th International Conference on Algorithms and Architectures for Parallel Processing - Volume Part I; 2012, p 114–128.

66. Smith DS, Gore JC, Yankeelov TE, Welch EB. Real-time compressive sensing MRI reconstruction using GPU computing and split Bregman methods. Int J Biomed Imaging 2012;2012:864827.

67. Bernstein MA, Zhou XJ, Polzin JA, et al. Concomitant gradient terms in phase contrast MR: Analysis and correction. Magn Reson Med 1998;39(2):300-308.

68. King KF, Ganin A, Zhou XJ, Bernstein MA. Concomitant gradient field effects in spiral scans. Magn Reson Med 1999;41(1):103-112.

69. Cheng JY, Santos JM, Pauly JM. Fast concomitant gradient field and field inhomogeneity correction for spiral cardiac imaging. Magn Reson Med 2011;66(2):390-401.

70. Barmet C, De ZN, Pruessmann KP. Spatiotemporal magnetic field monitoring for MR. Magn Reson Med 2008;60(1):187-197.

71. De Zanche N, Barmet C, Nordmeyer-Massner JA, Pruessmann KP. NMR probes for measuring magnetic fields and field dynamics in MR systems. Magn Reson Med 2008;60(1):176-186.

72. Wilm BJ, Barmet C, Pavan M, Pruessmann KP. Higher order reconstruction for MRI in the presence of spatiotemporal field perturbations. Magn Reson Med 2011;65(6):1690-1701.

73. https://github.com/ismrmrd/ismrmrd.

74. https://github.com/davidssmith/RawArray.jl.

75. Ravi KS, Potdar S, Poojar P, et al. Pulseq-graphical programming interface: Open source visual environment for prototyping pulse sequences and integrated magnetic resonance imaging algorithm development. Magn Reson Imaging 2018;52:9-15.

76. Barber NJ, Ako EO, Kowalik GT, et al. Magnetic resonance-augmented cardiopulmonary exercise testing. Circ Cardiovasc Imaging 2016;9(12):e005282.

77. Barral JK, Overall WR, Nystrom MM, et al. A novel platform for comprehensive CMR examination in a clinically feasible scan time. J Cardiovasc Magn Reson 2014;16(Suppl 1):W10.

78. Lim Y, Narayanan S, Nayak KS. Deblurring for spiral real-time MRI using convolutional neural networks. Magn Reson Med 2020;84:3438-3452.

79. Kakareka JW, Faranesh AZ, Pursley RH, et al. Physiological recording in the MRI environment (PRiME): MRI-compatible hemodynamic recording system. IEEE J Transl Eng Health Med 2018;6:4100112.

80. Rogers T, Ratnayaka K, Khan JM, et al. CMR fluoroscopy right heart catheterization for cardiac output and pulmonary vascular resistance: Results in 102 patients. J Cardiovasc Magn Reson 2017;19(1):54.

81. Inouye JM, Blemker SS, Inouye DI. Towards undistorted and noise-free speech in an MRI scanner: Correlation subtraction followed by spectral noise gating. J Acoust Soc Am 2014;135(3):1019-1022.

82. Santos JM, Wright GA, Pauly JM. Flexible real-time magnetic resonance imaging framework. Conf Proc IEEE Eng Med Biol Soc 2004;1: 1048-1051.

83. Guttman MA, Lederman RJ, Sorger JM, McVeigh ER. Real-time volume rendered MRI for interventional guidance. J Cardiovasc Magn Reson 2002;4(4):431-442.

84. Hatscher B, Mewes A, Pannicke E, et al. Touchless scanner control to support MRI-guided interventions. Int J Comput Assist Radiol Surg 2020;15(3):545-553.

85. Mewes A, Heinrich F, Hensen B, Wacker F, Lawonn K, Hansen C. Concepts for augmented reality visualisation to support needle guidance inside the MRI. Healthc Technol Lett 2018;5(5):172-176.

86. Unterberg-Buchwald C, Fasshauer M, Sohns JM, et al. Real time cardiac MRI and its clinical usefulness in arrhythmias and wall motion abnormalities. J Cardiovasc Magn Reson 2014;16(1):P34.

87. Allen BD, Carr ML, Markl M, et al. Accelerated real-time cardiac MRI using iterative sparse SENSE reconstruction: Comparing performance in patients with sinus rhythm and atrial fibrillation. Eur Radiol 2018;28 (7):3088-3096.

88. Ahmad R, Hu HH, Krishnamurthy R, Krishnamurthy R. Reducing sedation for pediatric body MRI using accelerated and abbreviated imaging protocols. Pediatr Radiol 2018;48(1):37-49.

89. Setser RM, Fischer SE, Lorenz CH. Quantification of left ventricular function with magnetic resonance images acquired in real time. J Magn Reson Imaging 2000;12(3):430-438.

90. Muthurangu V, Lurz P, Critchely JD, Deanfield JE, Taylor AM, Hansen MS. Real-time assessment of right and left ventricular volumes and function in patients with congenital heart disease by using high spatiotemporal resolution radial k-t SENSE. Radiology 2008;248(3):782-791.

91. Haji-Valizadeh H, Rahsepar AA, Collins JD, et al. Validation of highly accelerated real-time cardiac cine MRI with radial k-space sampling and compressed sensing in patients at 1.5T and 3T. Magn Reson Med 2018;79(5):2745-2751.

92. Voit D, Zhang S, Unterberg-Buchwald C, Sohns JM, Lotz J, Frahm J. Real-time cardiovascular magnetic resonance at 1.5 T using balanced SSFP and 40 msec resolution. J Cardiovasc Magn Reson 2013;15(1):79.

93. Hauptmann A, Arridge S, Lucka F, Muthurangu V, Steeden JA. Real-time cardiovascular MR with spatio-temporal artifact suppression using deep learning–proof of concept in congenital heart disease. Magn Reson Med 2019;81(2):1143-1156.

94. Kowalik GT, Knight D, Steeden JA, Muthurangu V. Perturbed spiral real-time phase-contrast MR with compressive sensing reconstruction for assessment of flow in children. Magn Reson Med 2020;83(6):2077-2091.

95. Roy CW, Seed M, Kingdom JC, Macgowan CK. Motion compensated cine CMR of the fetal heart using radial undersampling and compressed sensing. J Cardiovasc Magn Reson 2017;19(1):29.

96. Steeden JA, Kowalik GT, Tann O, Hughes M, Mortensen KH, Muthurangu V. Real-time assessment of right and left ventricular volumes and function in children using high spatiotemporal resolution spiral bSSFP with compressed sensing. J Cardiovasc Magn Reson 2018;20(1):79.

97. Tang C, Blatter DD, Parker DL. Accuracy of phase-contrast flow measurements in the presence of partial-volume effects. J Magn Reson Imaging 1993;3(2):377-385.

98. Gabbert DD, Hart C, Jerosch-Herold M, et al. Heart beat but not respiration is the main driving force of the systemic venous return in the Fontan circulation. Sci Rep 2019;9(1):2034.

99. Körperich H, Müller K, Barth P, et al. Differentiation of impaired from preserved hemodynamics in patients with Fontan circulation using real-time phase-velocity cardiovascular magnetic resonance. J Thorac Imaging 2017;32(3):159-168.

100. Hermann K, Jürgen G, Peter B, et al. Flow volume and shunt quantification in pediatric congenital heart disease by real-time magnetic resonance velocity mapping. Circulation 2004;109(16):1987-1993.

101. Kowallick JT, Joseph AA, Unterberg-Buchwald C, et al. Real-time phase-contrast flow MRI of the ascending aorta and superior vena cava as a function of intrathoracic pressure (Valsalva manoeuvre). Br J Radiol 2014;87(1042):20140401.

102. Singh JP, Larson MG, Manolio TA, et al. Blood pressure response during treadmill testing as a risk factor for new-onset hypertension. Circulation 1999;99(14):1831-1836.

103. Lurz P, Muthurangu V, Schuler PK, et al. Impact of reduction in right ventricular pressure and/or volume overload by percutaneous pulmonary valve implantation on biventricular response to exercise: An exercise stress real-time CMR study. Eur Heart J 2012;33(19):2434-2441.

104. O'Meagher S, Munoz PA, Muthurangu V, et al. Mechanisms of maintained exercise capacity in adults with repaired tetralogy of Fallot. Int J Cardiol 2014;177(1):178-181.

105. Jaijee S, Quinlan M, Tokarczuk P, et al. Exercise cardiac MRI unmasks right ventricular dysfunction in acute hypoxia and chronic pulmonary arterial hypertension. Am J Physiol Circ Physiol 2018;315(4):H950-H957.

106. Hjortdal VE, Emmertsen K, Stenbøg E, et al. Effects of exercise and respiration on blood flow in total cavopulmonary connection. Circulation 2003;108(10):1227-1231.

107. Pedersen LM, Pedersen TAL, Pedersen EM, Højmyr H, Emmertsen K, Hjortdal VE. Blood flow measured by magnetic resonance imaging at rest and exercise after surgical bypass of aortic arch obstruction. Eur J Cardio-Thoracic Surg 2010;37(3):658-661.

108. Barber NJ, Ako EO, Kowalik GT, Steeden JA, Pandya B, Muthurangu V. MR augmented cardiopulmonary exercise testing—A novel approach to assessing cardiovascular function. Physiol Meas 2015;36(5):N85-N94.

109. Manganaro L, Savelli S, Di Maurizio M, et al. Potential role of fetal cardiac evaluation with magnetic resonance imaging: Preliminary experience. Prenat Diagn 2008;28(2):148-156.

110. Roy CW, van Amerom JFP, Marini D, Seed M, Macgowan CK. Fetal cardiac MRI: A review of technical advancements. Top Magn Reson Imaging 2019;28(5):235-244.

111. Mukherjee RK, Chubb H, Roujol S, Razavi R, O'Neill MD. Advances in real-time MRI-guided electrophysiology. Curr Cardiovasc Imaging Rep 2019;12(2):6.

112. Campbell-Washburn AE, Tavallaei MA, Pop M, et al. Real-time MRI guidance of cardiac interventions. J Magn Reson Imaging 2017;46(4):935-950.

113. Campbell-Washburn AE, Faranesh AZ, Lederman RJ, Hansen MS. Magnetic resonance sequences and rapid acquisition for MR-guided interventions. Magn Reson Imaging Clin N Am 2015;23(4):669-679.

114. Chubb H, Harrison JL, Weiss S, et al. Development, preclinical validation, and clinical translation of a cardiac magnetic resonance-electrophysiology system with active catheter tracking for ablation of cardiac arrhythmia. JACC Clin Electrophysiol 2017;3(2):89-103.

115. Ratnayaka K, Kanter JP, Faranesh AZ, et al. Radiation-free CMR diagnostic heart catheterization in children. J Cardiovasc Magn Reson 2017;19(1):65.

116. Toupin S, Bour P, Lepetit-Coiffé M, et al. Feasibility of real-time MR thermal dose mapping for predicting radiofrequency ablation outcome in the myocardium in vivo. J Cardiovasc Magn Reson 2017;19(1):14.

117. Penzkofer T, Tuncali K, Fedorov A, et al. Transperineal in-bore 3-T MR imaging-guided prostate biopsy: A prospective clinical observational study. Radiology 2014;274(1):170-180.

118. van den Bosch MAAJ, Daniel BL, Pal S, et al. MRI-guided needle localization of suspicious breast lesions: Results of a freehand technique. Eur Radiol 2006;16(8):1811-1817.

119. Mittauer K, Paliwal B, Hill P, et al. A new era of image guidance with magnetic resonance-guided radiation therapy for abdominal and thoracic malignancies. Cureus 2018;10(4):e2422.

120. van den Bosch M, Daniel B, Rieke V, Butts-Pauly K, Kermit E, Jeffrey S. MRI-guided radiofrequency ablation of breast cancer: Preliminary clinical experience. J Magn Reson Imaging 2008;27(1):204-208.

121. Lewin JS, Nour SG, Connell CF, et al. Phase II clinical trial of interactive MR imaging–guided interstitial radiofrequency thermal ablation of primary kidney tumors: Initial experience. Radiology 2004;232(3):835-845.

122. Woodrum DA, Kawashima A, Gorny KR, Mynderse LA. Magnetic resonance-guided thermal therapy for localized and recurrent prostate cancer. Magn Reson Imaging Clin N Am 2015;23(4):607-619.

123. Zippel DB, Papa MZ. The use of MR imaging guided focused ultrasound in breast cancer patients; a preliminary phase one study and review. Breast Cancer 2005;12(1):32-38.

124. Grothoff M, Piorkowski C, Eitel C, et al. MR imaging–guided electrophysiological ablation studies in humans with passive catheter tracking: Initial results. Radiology 2014;271(3):695-702.

125. Sommer P, Grothoff M, Eitel C, et al. Feasibility of real-time magnetic resonance imaging-guided electrophysiology studies in humans. Europace 2012;15(1):101-108.

126. Pushparajah K, Tzifa A, Razavi R. Cardiac MRI catheterization: A 10-year single institution experience and review. Interv Cardiol 2014;6(3):335-346.

127. Sonmez M, Saikus CE, Bell JA, et al. MRI active guidewire with an embedded temperature probe and providing a distinct tip signal to enhance clinical safety. J Cardiovasc Magn Reson 2012;14(1):38.

128. Dumoulin CL, Souza SP, Darrow RD. Real-time position monitoring of invasive devices using magnetic resonance. Magn Reson Med 1993;29(3):411-415.

129. Sathyanarayana S, Schär M, Kraitchman DL, Bottomley PA. Towards real-time intravascular endoscopic magnetic resonance imaging. JACC Cardiovasc Imaging 2010;3(11):1158-1165.

130. Scheer JK, Hamelin T, Chang L, Lemkuil B, Carter BS, Chen CC. Real-time magnetic resonance imaging-guided biopsy using SmartFrame® stereotaxis in the setting of a conventional diagnostic magnetic resonance imaging suite. Oper Neurosurg 2017;13(3):329-337.

131. Moche M, Heinig S, Garnov N, et al. Navigated MRI-guided liver biopsies in a closed-bore scanner: Experience in 52 patients. Eur Radiol 2016;26(8):2462-2470.

132. Overduin CG, Heidkamp J, Rothgang E, Barentsz JO, de Lange F, Fütterer JJ. Fast 3-T MR-guided transrectal prostate biopsy using an in-room tablet device for needle guide alignment: A feasibility study. Eur Radiol 2018;28(11):4824-4831.

133. Heidt T, Reiss S, Krafft AJ, et al. Real-time magnetic resonance imaging-guided coronary intervention in a porcine model. Sci Rep 2019;9(1):8663.

134. Campbell-Washburn AE, Rogers T, Stine AM, et al. Right heart catheterization using metallic guidewires and low SAR cardiovascular magnetic resonance fluoroscopy at 1.5 Tesla: First in human experience. J Cardiovasc Magn Reson 2018;20(1):41.

135. Unterberg-Buchwald C, Ritter CO, Reupke V, et al. Targeted endomyocardial biopsy guided by real-time cardiovascular magnetic resonance. J Cardiovasc Magn Reson 2017;19(1):45.

136. Ozenne V, Toupin S, Bour P, et al. Improved cardiac magnetic resonance thermometry and dosimetry for monitoring lesion formation during catheter ablation. Magn Reson Med 2017;77(2):673-683.

137. Kim T, Park JC, Gach HM, Chun J, Mutic S. Technical note: Real-time 3D MRI in the presence of motion for MRI-guided radiotherapy: 3D dynamic keyhole imaging with super-resolution. Med Phys 2019;46 (10):4631-4638.

138. Chen W, Byrd D, Narayanan S, Nayak KS. Intermittently tagged real-time MRI reveals internal tongue motion during speech production. Magn Reson Med 2019;82(2):600-613.

139. Chen W, Lee NG, Byrd D, Narayanan S, Nayak KS. Improved real-time tagged MRI using REALTAG. Magn Reson Med 2020;84(2):838-846.

140. Zhu Y, Kim YC, Proctor MI, Narayanan SS, Nayak KS. Dynamic 3-D visualization of vocal tract shaping during speech. IEEE Trans Med Imaging 2013;32(5):838-848.

141. Engwall O. From real-time MRI to 3D tongue movements. Interspeech 2004;1:1109-1112.

142. Lingala SG, Toutios A, Toger J, Lim Y, Zhu Y, Kim YC, et al. State-of-the-art MRI protocol for comprehensive assessment of vocal tract structure and function. In: Proc Interspeech; 2016, p 475–9.

143. Olthoff A, Joseph AA, Weidenmüller M, Riley B, Frahm J. Real-time MRI of swallowing: Intraoral pressure reduction supports larynx elevation. NMR Biomed 2016;29(11):1618-1623.

144. Scott AD, Wylezinska M, Birch MJ, Miquel ME. Speech MRI: Morphology and function. Phys Medica 2014;30(6):604-618.

145. Nayak KS, Fleck RJ. Seeing sleep: Dynamic imaging of upper airway collapse and collapsibility in children. IEEE Pulse 2014;5(5):40-44.

146. Bresch E, Nielsen J, Nayak K, Narayanan S. Synchronized and noise-robust audio recordings during realtime magnetic resonance imaging scans. J Acoust Soc Am 2006;120(4):1791-1794.

147. Tian W, Li Y, Yin H, et al. Magnetic resonance imaging assessment of velopharyngeal motion in Chinese children after primary palatal repair. J Craniofac Surg 2010;21(2):578-587.

148. Hagedorn C, Lammert A, Zu Y, Sinha U, Goldstein L, Narayanan SS. Characterizing post-glossectomy speech using real-time magnetic resonance imaging. J Acoust Soc Am 2013;134(5):4205.

149. Mady K, Sader R, Beer A, Hoole P, Zimmermann A, Hannig C. Consonant articulation in glossectomee speech evaluated by dynamic MRI. In: Proceedings of the Fifteenth International Congress of Phonetic Sciences (ICPhS); 2015, p 3233–3236.

150. Bae Y, Kuehn DP, Conway CA, Sutton BP. Real-time magnetic resonance imaging of velopharyngeal activities with simultaneous speech recordings. Cleft Palate-Craniofacial J 2011;48(6):695-707.

151. Kazan-Tannus JF, Levine D, McKenzie C, et al. Real-time magnetic resonance imaging aids prenatal diagnosis of isolated cleft palate. J Ultrasound Med 2005;24(11):1533-1540.

152. Bresch E, Kim Y-C, Nayak K, Byrd D, Narayanan S. Seeing speech: Capturing vocal tract shaping using real-time magnetic resonance imaging [exploratory DSP]. IEEE Signal Process Mag 2008;25(3): 123-132.

153. Kim Y-C. Fast upper airway magnetic resonance imaging for assessment of speech production and sleep apnea. Precis Futur Med 2018; 2(4):131-148.

154. Ramanarayanan V, Tilsen S, Proctor M, et al. Analysis of speech production real-time MRI. Comput Speech Lang 2018;52:1-22.

155. Zhang S, Joseph AA, Gross L, Ghadimi M, Frahm J, Beham AW. Diagnosis of gastroesophageal reflux disease using real-time magnetic resonance imaging. Sci Rep 2015;5(1):12112.

156. Freitas AC, Ruthven M, Boubertakh R, Miquel ME. Real-time speech MRI: Commercial Cartesian and non-Cartesian sequences at 3T and feasibility of offline TGV reconstruction to visualise velopharyngeal motion. Phys Medica 2018;46:96-103.

157. Uecker M, Zhang S, Voit D, Karaus A, Merboldt KD, Frahm J. Real-time MRI at a resolution of 20 msec. NMR Biomed 2010;23(8): 986-994.

158. Niebergall A, Zhang S, Kunay E, et al. Real-time MRI of speaking at a resolution of 33 msec: Undersampled radial FLASH with nonlinear inverse reconstruction. Magn Reson Med 2013;69(2):477-485.

159. Iltis PW, Frahm J, Voit D, Joseph AA, Schoonderwaldt E, Altenmüller E. High-speed real-time magnetic resonance imaging of fast tongue movements in elite horn players. Quant Imaging Med Surg 2015;5(3):374-381.

160. Sutton BP, Conway CA, Bae Y, Seethamraju R, Kuehn DP. Faster dynamic imaging of speech with field inhomogeneity corrected spiral fast low angle shot (FLASH) at 3 T. J Magn Reson Imaging 2010;32(5): 1228-1237.

161. Lim Y, Lingala SG, Narayanan SS, Nayak KS. Dynamic off-resonance correction for spiral real-time MRI of speech. Magn Reson Med 2019; 81(1):234-246.

162. Feng X, Blemker SS, Inouye J, Pelland CM, Zhao L, Meyer CH. Assessment of velopharyngeal function with dual-planar high-resolution real-time spiral dynamic MRI. Magn Reson Med 2018;80: 1467-1474.

163. Borotikar B, Lempereur M, Lelievre M, Burdin V, Ben Salem D, Brochard S. Dynamic MRI to quantify musculoskeletal motion: A systematic review of concurrent validity and reliability, and perspectives for evaluation of musculoskeletal disorders. PLoS One 2017;12(12): e0189587-e0189587.

164. Fiorentino NM, Lin JS, Ridder KB, Guttman MA, McVeigh ER, Blemker SS. Rectus femoris knee muscle moment arms measured in vivo during dynamic motion with real-time magnetic resonance imaging. J Biomech Eng 2013;135(4):044501.

165. Shaw CB, Foster BH, Borgese M, et al. Real-time three-dimensional MRI for the assessment of dynamic carpal instability. PLoS One 2019; 14(9):e0222704.

166. Krohn S, Gersdorff N, Wassmann T, et al. Real-time MRI of the temporomandibular joint at 15 frames per second—A feasibility study. Eur J Radiol 2016;85(12):2225-2230.

167. d'Entremont AG, Nordmeyer-Massner JA, Bos C, Wilson DR, Pruessmann KP. Do dynamic-based MR knee kinematics methods produce the same results as static methods? Magn Reson Med 2013;69 (6):1634-1644.

168. Kaiser J, Bradford R, Johnson K, Wieben O, Thelen DG. Measurement of tibiofemoral kinematics using highly accelerated 3D radial sampling. Magn Reson Med 2013;69(5):1310-1316.

169. Mazzoli V, Oudeman J, Nicolay K, et al. Assessment of passive muscle elongation using diffusion tensor MRI: Correlation between fiber length and diffusion coefficients. NMR Biomed 2016;29(12):1813-1824.

170. Deligianni X, Pansini M, Garcia M, et al. Synchronous MRI of muscle motion induced by electrical stimulation. Magn Reson Med 2017;77 (2):664-672.

171. Westphal CJ, Schmitz A, Reeder SB, Thelen DG. Load-dependent variations in knee kinematics measured with dynamic MRI. J Biomech 2013;46(12):2045-2052.

172. Quick HH, Ladd ME, Hoevel M, et al. Real-time MRI of joint movement with trueFISP. J Magn Reson Imaging 2002;15(6):710-715.

173. Mazzoli V, Nederveen AJ, Oudeman J, et al. Water and fat separation in real-time MRI of joint movement with phase-sensitive bSSFP. Magn Reson Med 2017;78(1):58-68.

174. Tan Z, Voit D, Kollmeier JM, Uecker M, Frahm J. Dynamic water/fat separation and inhomogeneity mapping—Joint estimation using undersampled triple-echo multi-spoke radial FLASH. Magn Reson Med 2019;82(3):1000-1011.

175. Draper CE, Santos JM, Kourtis LC, et al. Feasibility of using real-time MRI to measure joint kinematics in 1.5T and open-bore 0.5T systems. J Magn Reson Imaging 2008;28(1):158-166.

176. Draper CE, Besier TF, Santos JM, et al. Using real-time MRI to quantify altered joint kinematics in subjects with patellofemoral pain and to evaluate the effects of a patellar brace or sleeve on joint motion. J Orthop Res 2009;27(5):571-577.

177. Draper CE, Besier TF, Fredericson M, et al. Differences in patellofemoral kinematics between weight-bearing and non-weight-bearing conditions in patients with patellofemoral pain. J Orthop Res 2011;29(3):312-317.

178. Lin C-C, Zhang S, Hsu C-Y, Frahm J, Lu T-W, Shih T-F. Measuring three-dimensional tibiofemoral kinematics using dual-slice real-time magnetic resonance imaging. Med Phys 2019;46(10):4588-4599.

179. Lin C-C, Zhang S, Frahm J, Lu T-W, Hsu C-Y, Shih T-F. A slice-to-volume registration method based on real-time magnetic resonance imaging for measuring three-dimensional kinematics of the knee. Med Phys 2013;40(10):102302.

180. Kawchuk GN, Fryer J, Jaremko JL, Zeng H, Rowe L, Thompson R. Real-time visualization of joint cavitation. PLoS One 2015;10(4): e0119470.

181. Henrichon SS, Foster BH, Shaw C, et al. Dynamic MRI of the wrist in less than 20 seconds: Normal midcarpal motion and reader reliability. Skeletal Radiol 2020;49(2):241-248.

182. Tempelaere C, Pierrart J, Lefèvre-Colau M-M, et al. Dynamic three-dimensional shoulder MRI during active motion for investigation of rotator cuff diseases. PLoS One 2016;11(7):e0158563.

183. Yen P, Katzberg RW, Buonocore MH, Sonico J. Dynamic MR imaging of the temporomandibular joint using a balanced steady-state free precession sequence at 3T. Am J Neuroradiol 2013;34(3):E24-E26.

184. Menys A, Taylor SA, Emmanuel A, et al. Global small bowel motility: Assessment with dynamic MR imaging. Radiology 2013;269(2): 443-450.

185. de Jonge CS, Coolen BF, Peper ES, et al. Evaluation of compressed sensing MRI for accelerated bowel motility imaging. Eur Radiol Exp 2019;3(1):7.

186. Seif Amir Hosseini A, Uhlig J, Streit U, et al. Real-time MRI for the dynamic assessment of fundoplication failure in patients with gastro-esophageal reflux disease. Eur Radiol 2019;29(9):4691-4698.

187. Rai R, Sidhom M, Lim K, Ohanessian L, Liney GP. MRI micturating urethrography for improved urethral delineation in prostate radiotherapy planning: A case study. Phys Med Biol 2017;62(8):3003-3010.

188. Maccioni F. Functional disorders of the ano-rectal compartment of the pelvic floor: Clinical and diagnostic value of dynamic MRI. Abdom Imaging 2013;38(5):930-951.

189. Maccioni F, Alt CD. MRI of the pelvic floor and MR defecography. In: Hodler J, Kubik-Huch RA, von Schulthess GK, editors. *Diseases of the abdomen and pelvis 2018–2021: IDKD Springer Series*. Cham, Switzerland: Springer; 2018. p 13-20.

190. Kubik-Huch RA, Wisser J, Stallmach T, Ladd ME, Meier A, Marincek B. Prenatal diagnosis of fetal malformations by ultrafast magnetic resonance imaging. Prenat Diagn 1998;18(11):1205-1208.

191. Guo W-Y, Wong T-T. Screening of fetal CNS anomalies by MR imaging. Childs Nerv Syst 2003;19(7):410-414.

192. Levine D, Cavazos C, Kazan-Tannus JF, et al. Evaluation of real-time single-shot fast spin-echo MRI for visualization of the fetal midline corpus callosum and secondary palate. Am J Roentgenol 2006;187(6): 1505-1511.

193. Yankeelov TE, Gore JC. Dynamic contrast enhanced magnetic resonance imaging in oncology: Theory, data acquisition, analysis, and examples. Curr Med Imaging Rev 2009;3(2):91-107.

194. Riederer SJ, Haider CR, Borisch EA, Weavers PT, Young PM. Recent advances in 3D time-resolved contrast-enhanced MR angiography. J Magn Reson Imaging 2015;42(1):3-22.

195. van Osch MJP, Teeuwisse WM, Chen Z, Suzuki Y, Helle M, Schmid S. Advances in arterial spin labelling MRI methods for measuring perfusion and collateral flow. J Cereb Blood Flow Metab 2017;38(9):1461-1480.

196. Hennig J, Zhong K, Speck O. MR-encephalography: Fast multi-channel monitoring of brain physiology with magnetic resonance. Neuroimage 2007;34(1):212-219.

197. Li X, Young AS, Raman SS, et al. Automatic needle tracking using mask R-CNN for MRI-guided percutaneous interventions. Int J Comput Assist Radiol Surg 2020;15:1673-1684.

198. Zhou Z, Han F, Ghodrati V, et al. Parallel imaging and convolutional neural network combined fast MR image reconstruction: Applications in low-latency accelerated real-time imaging. Med Phys 2019;46(8): 3399-3413.

199. Han F, Zhou Z, Kouzehkonan VG, Gao Y, Yang Y, Hu P. Single breath-held, ECG-free cardiac CINE MRI using parallel imaging and deep learning combined image reconstruction. In: Proc 27th Annual Meeting of ISMRM, Montréal; 2019, p 1048.

200. Dietz B, Fallone G, Wachowicz K. Real-time MR image reconstruction using convolutional neural networks. In: Proc 27th Annual Meeting of ISMRM, Montréal; 2019, p 4784.

201. Alkan C, Fang Z, Lee JH. Convolutional neural network for real-time high spatial resolution functional magnetic resonance imaging. In: Proc 27th Annual Meeting of ISMRM, Montréal; 2019, p 4792.

202. Saha P, Srungarapu P, Fels S. Towards automatic speech identification from vocal tract shape dynamics in real-time MRI. In: Proc Interspeech; 2018, p 1249–1253.

203. Leeuwen KG van, Bos P, Trebeschi S, Alphen MJA van, Voskuilen L, Smeele LE, et al. CNN-based phoneme classifier from vocal tract MRI learns embedding consistent with articulatory topology. In: Proc Interspeech; 2019, p 909–913.

204. Somandepalli K, Toutios A, Narayanan SS. Semantic edge detection for tracking vocal tract air-tissue boundaries in real-time magnetic resonance images. In: Proc Interspeech; 2017, p 631–635.

205. Valliappan CA, Mannem R, Ghosh PK. Air-tissue boundary segmentation in real-time magnetic resonance imaging video using semantic segmentation with fully convolutional networks. In: Proc Interspeech; 2018, p 3132–3136.

206. Yang F, Zhang Y, Lei P, et al. A deep learning segmentation approach in free-breathing real-time cardiac magnetic resonance imaging. Biomed Res Int 2019;2019:5636423.

207. Weine J, Breton E, Garnon J, Gangi A, Maier F. Deep learning-based needle localization on real-time MR images of patients acquired during MR-guided percutaneous interventions. In: Proc 27th Annual Meeting of ISMRM, Montréal; 2019, p 0973.

208. Krishnamurthy D, You W, Kapse K, Limperopoulos C. Real-time ultrafast fetal brain localization using convolutional neural networks. In: Proc 27th Annual Meeting of ISMRM, Montréal; 2019, p 4810.

209. Kim J-M, Jeong Y-J, Cheong H-J, Yoo J-W, Kim J-H, Lee C, et al. Real-time T1/PRF-based MR thermometry using deep learning and VFA-mFFE for guidance of HIFU treatment. In: Proc 27th Annual Meeting of ISMRM, Montréal; 2019, p 0970.

210. https://www.heartvista.ai/technology.

211. https://www.mevis.fraunhofer.de/en/solutionpages/deep-learning-in-medical-imaging.html.

212. Campbell-Washburn AE, Ramasawmy R, Restivo MC, et al. Opportunities in interventional and diagnostic imaging by using high-performance low-field-strength MRI. Radiology 2019;293(2):384-393.

213. Konings MK, Bartels LW, Smits HFM, Bakker CJG. Heating around intravascular guidewires by resonating RF waves. J Magn Reson Imaging 2000;12(1):79-85.

214. Wald LL, McDaniel PC, Witzel T, Stockmann JP, Cooley CZ. Low-cost and portable MRI. J Magn Reson Imaging 2020;52:686-696.